Interplay between intrinsic and emergent topological protection on interacting helical modes

Raul A. Santos,[1,2] D. B. Gutman,[3] and Sam T. Carr[4]

[1]*T.C.M. Group, Cavendish Laboratory, University of Cambridge, J.J. Thomson Avenue, Cambridge, CB3 0HE, United Kingdom*

[2]*School of Physics & Astronomy, University of Birmingham, Edgbaston, Birmingham, B15 2TT, United Kingdom*

[3]*Department of Physics, Bar-Ilan University, Ramat Gan, 52900, Israel*

[4]*School of Physical Sciences, University of Kent, Canterbury CT2 7NH, United Kingdom*

(Received 14 June 2018; published 14 February 2019)

The interplay between topology and interactions on the edge of a two-dimensional topological insulator with time-reversal symmetry is studied. We consider a simple noninteracting system of three helical channels with an inherent $\mathbb{Z}_2$ topological protection and hence a zero-temperature conductance of $G = e^2/h$. We show that when interactions are added to the model, the ground state exhibits two different phases as a function of the interaction parameters. One of these phases is a trivial insulator at zero temperature, as the symmetry protecting the noninteracting topological phase is spontaneously broken. In this phase there is zero conductance ($G = 0$) at zero temperature. The other phase displays enhanced topological properties, with a topologically protected zero-temperature conductance of $G = 3e^2/h$ and an emergent $\mathbb{Z}_3$ symmetry not present in the lattice model. The neutral sector in this phase is described by a massive version of $\mathbb{Z}_3$ parafermions. This state is an example of a dynamically enhanced symmetry-protected topological state.

DOI: 10.1103/PhysRevB.99.075129

I. INTRODUCTION

Topology plays a central role in the modern understanding of different physical systems, ranging from superfluid helium to elementary particles [1–3]. In the context of solid-state physics, one of the first phenomenon that was identified as having a topological origin was the integer quantum Hall effect (IQHE). In the IQHE, the existence of protected chiral modes on the edge of the sample is a consequence of the existence of a nontrivial first Chern number [4]. The topological nature of these modes renders them robust against disorder and enforces a quantization of the conductance in units e^2/h, where h is the Planck constant and e the electric charge. The inclusion of interactions dramatically changes this picture, as occurs in the fractional quantum Hall effect (FQHE), where the huge degeneracy between fractionally filled many-body states is (partly) lifted by the interaction, creating a correlated state with fractional conductance and exotic quasiparticles [5,6].

In recent years, time-reversal (TR) invariant topological materials were discovered, reviving interest in topological systems. Examples of such topological insulators (TIs) are formed due to a spin-orbit interaction [7–18] that is sufficiently strong to invert the s-like valence electronic states and p-like conduction electrons in different heterostructures [11,19]. For noninteracting disordered systems, a topological classification has been fully established [20,21] and is uniquely determined by the symmetry class and dimensionality of the single-particle Hamiltonian.

In particular, in two spatial dimensions noninteracting TIs display helical edge modes. The parity of the number of edge modes in these TIs is a $\mathbb{Z}_2$ topological invariant. The electric conductance of a noninteracting TI is fixed as long as TR symmetry is preserved, due to the destructive interference between the counterpropagating spin states around a nonmagnetic impurity. The role of symmetry in these states is crucial to preserve the topological properties. It is for this reason that they are dubbed symmetry-protected topological (SPT) states.

Weak interactions can change the topological properties of a noninteracting system in different ways, e.g., by modifying the whole state including the bulk, or by changing the edge degrees of freedom in the system without changing the overall structure in the bulk. An example of the former corresponds to the interacting Kitaev chain [22], where the inclusion of interactions allows the adiabatic connection of two Hamiltonians belonging to different noninteracting topological states, reducing the noninteracting classification of $\mathbb{Z}$ down to $\mathbb{Z}_8$. On the other hand, when the characteristic interaction strength is smaller than the bulk gap energy, interactions can only induce a change at the edge degrees of freedom. In this latter context, it has been recently found that the interactions may lead to an emergence of topologically nontrivial edge states in systems that are topologically trivial on the bulk according to the noninteracting classification.

The simplest example of this kind of phenomena appears on the edge of a two-dimensional TI supporting two parallel helical modes. Generically, in a noninteracting system, these modes can hybridize and be localized by the presence of a sufficiently high density of impurities, making the system topologically trivial. Surprisingly, in the presence of interparticle interactions there is some possibility for these modes to be protected against localization, by a zero bias anomaly mechanism in the case of vanishing tunneling [23] or by the emergence of an effective spin gap [24,25] that suppresses single-particle backscattering when tunneling is present. In these cases, the system displays topological signatures, for example, a robust value of conductance quantized in units of e^2/h, and fractionalized zero modes in domain wall

configurations. This protection has also been predicted to appear in truly one-dimensional systems with spin-orbit interaction [26,27].

Another mechanism in which interactions can affect the topological properties of a nontrivial SPT state is by inducing a spontaneous breaking of the protecting symmetry in the ground state, rendering the state topologically trivial. Recently [28], it has been shown that in a general system of $N > 2$ helical modes, interactions can decrease the conductance of the system to zero at zero temperature by creating a ground state that spontaneously breaks TR symmetry.

In this work, we focus on a system of three coupled helical modes with interchannel tunneling, corresponding to the edge structure of an integer TI. This edge-mode arrangement can appear when single-edge-mode TIs are stacked, or when the confining potential in a sample induces an edge reconstruction. Because the number of modes is odd, this system is topologically nontrivial according to the noninteracting classification, and disorder can localize two modes at most, leaving one helical mode free to carry the charge. We show that the interactions generate two distinct phases in which each of the effects discussed above can occur: in one phase, the intrinsic topology is destroyed due to the spontaneous breaking of TR symmetry, while in the other phase, the inherent topological protection is enhanced through a distinct emergent topological state that protects all three helical modes against localization. Both of these states have a number of emergent energy scales with different characteristics, which we summarize below.

A. Summary of main results

Before delving into the technical details of the analysis, it is worth listing the main results that we find in this paper. The model of three coupled helical edges is developed in Sec. II and illustrated schematically in Fig. 2. The noninteracting system consists of three helical edge modes, which could arise by stacking quantum-spin-Hall insulators (see [29–31] for related discussions in the context of quantum Hall systems), or alternatively, from the reconstruction of edge states in a single quantum-spin-Hall insulator (which is known to occur also in quantum Hall systems, see, e.g., [32,33]). The essential feature is that in the clean noninteracting system, there are three helical modes, from which one of them is topologically protected against localization due to the intrinsic $\mathbb{Z}_2$ topology dictated by the TR symmetry of the model.

Our results consider the fate of this system when weak interactions are introduced. We find that two distinct phases may develop, corresponding to:

(1) An emergent topological (ET) state, whose topology differs from the intrinsic topology of three channels. In this ET state all three edge modes are protected against localization when the disorder is added to the system, meaning that the low-temperature conductance is $G = 3e^2/h$; and

(2) A state that is characterized by time-reversal symmetry breaking (TRSB) in the ground state which destroys the intrinsic topology (that was protected by TR symmetry) and leads to a vanishing low-temperature conductance.

The different phases of the system are determined by the relative strength of the intra- and intermode interactions. The phase diagram of the model is displayed in Figs. 4 and 5 later in the paper and shows that the generic scenario of intrachain interactions being repulsive and stronger than interchain interactions (which are also repulsive) corresponds to the TRSB phase. However, the phase diagram also shows that even within purely repulsive interactions, either phase is possible in the presence of tunneling between the channels, indicating that details of the edge in any given realization of the system are crucial to determine the fate of the interacting system.

The TRSB and the ET phases share some commonalities. Their low-energy excitations (in the clean system) correspond to a gapless plasmon mode and neutral excitations with a gap Δ_n. Both states display the phenomenon of dynamical symmetry enhancement, whereby the symmetry of the ground state is higher than in the original problem. Both fixed points can be obtained via an adiabatic deformation of the SU(3) Gross-Neveu model, which ultimately has a $\mathbb{Z}_3$ symmetry. It is worth stressing that this is true even though the microscopic model **does not** possess this symmetry.

We now summarize the physical properties of each of the states. First, in the TRSB state:

(1) The ground state can be described by quasi-long-range order parameters. The dominant one is controlled by details of the interaction and can be either two-particle or trionic. One can picture this state as a sliding charge-density wave.

(2) Nonmagnetic impurities in the TRSB phase become spontaneously magnetic due to the spontaneous breaking of TR symmetry in the ground state. This means that an impurity that is initially even under TR symmetry, acquires an odd part when the system enters the TRSB phase. This mechanism and the presence of impurities renders the phase insulating at low energies. This is schematically shown in Fig. 7.

(3) In the clean TRSB phase, the system possesses a gapless plasmon mode that renders all order parameters quasi-long-range ordered. In the presence of disorder or an appropriate Umklapp scattering, if the Fermi momenta of the different modes have the correct commensurability relationship, the charge mode is gapped and the order parameter becomes nonzero.

Turning now to the phase with emergent topology:

(1) The ground state is a $\mathbb{Z}_3$ symmetry-protected topological state, where we stress again that the $\mathbb{Z}_3$ symmetry is itself emergent and therefore the lattice model itself is not required to (and in general does not) have this symmetry.

(2) The phase boundary between the ET phase and the TRSB phase is described by a critical theory that belongs to the same universality class as the three-state Potts model, corresponding in the continuous limit to a conformal field theory (CFT) with central charge $c = 4/5$ and $\mathbb{Z}_3$ parafermionic low-energy modes.

(3) At temperatures above the neutral gap, the conductance may drop below $3e^2/h$, while it will recover to the full quantum conductance $G = 3e^2/h$ at low temperature. A schematic diagram of this is plotted in Fig. 7.

All the previous points highlight that while the characterization of the conductance in the ground state of each phase is a property to consider, it does not capture all the physical features of the system.

This article develops as follows: In Sec. II we introduce a simple phenomenological model for three helical states in the

clean case, having in mind a realization based on three stacked TIs. The model in this section displays the general features of this system. We first describe the single-particle Hamiltonian and then introduce generic interactions. In Sec. III we analyze the low-energy or infrared (IR) description of the system in terms of Abelian and non-Abelian bosonization. Here we find that the neutral sector is represented by an adiabatic deformation of an emergent SU(3) symmetry. We analyze the structure of all two-particle operators that represent backscattering and introduce the relevant order parameters in the TRSB and ET phases in IV. In Sec. V we discuss the stability of the phases against general interaction terms. Following this analysis, in Sec. VI we discuss the transition between the TRSB and ET phase. To gain further insight we develop an intuition about the structure of the massive degrees of freedom in terms of an effective parafermionic model on the lattice that respects all the symmetries of the continuous model. Here we show that in the transition region between topological to trivial phase along the edge, a parafermionic mode is trapped in the domain wall. In Sec. VII we discuss the fate of disorder in the system, showing the difference between these phases. Finally, in Sec. VIII we discuss the results and present our conclusions.

II. THE MODEL

A. Single-particle Hamiltonian

While no symmetry apart from TR symmetry should be expected on the edge of a multichannel TR topological insulator, to keep the exposition and the relation to the physical regimes clear, here we consider a simple model that displays all the features of the generic model. We assume that the system consists of three TIs stacked in parallel, giving rise to three edge modes with approximately similar parameters. To simplify the analysis we focus on the limit of identical edge modes. A small asymmetry between the modes does not significantly modify the results. This discussion is presented in Appendix A. The electrons in the helical modes we consider are described by the fermion destruction $c^{\eta}_{k,a}$ and creation $(c^{\eta}_{k,a})^{\dagger}$ operators; k denotes the electron momentum and is assumed to be in the vicinity of the Fermi point. $a = (1, 2, 3)$ denotes the mode and $\eta = (+, -)$ labels its helicity. For small momenta, the noninteracting single-particle Hamiltonian is

$$H_0 = \sum_{k,a,\eta} \epsilon_{\eta}(k) n_{k,a} - \frac{t_{\perp}}{\sqrt{2}} \sum_{k,\eta} \left[\left(c^{\eta}_{k,2}\right)^{\dagger} \left(c^{\eta}_{k,1} + c^{\eta}_{k,3}\right) + \text{H.c.} \right], \tag{1}$$

where $\epsilon_{\eta}(k) = \eta v_F k$ is the linearized energy of each helical mode around the Fermi energy. We assume that the Fermi velocities v_F of all the modes coincide, which is a natural assumption in the case of three similar stacked TIs. In the case of edge reconstruction, this assumption is less justified, but as we discuss in Appendix A, the presence of a gap due to interactions in a sector of the theory makes small velocity differences irrelevant. The operator $n_{k,a} = (c^{\eta}_{k,a})^{\dagger} c^{\eta}_{k,a}$ measures the number of modes of helicity η and momentum k. The parameter $t_{\perp}$ describes the tunneling amplitude between different modes of the same helicity. Here we assume that tunneling occurs only between the modes which are closest in space. A diagram of the arrangement of helical modes and their labels is given in Fig. 1. Note that although tunneling between Kramers pairs is forbidden by TR symmetry, tunneling between modes of the same helicity is not constrained. Generically, this tunneling will exist and will be nonuniversal. In this section, we assume that it takes the simple form given by the second term in Eq. (1). A more general tunneling term does not change the overall picture (see Appendix A).

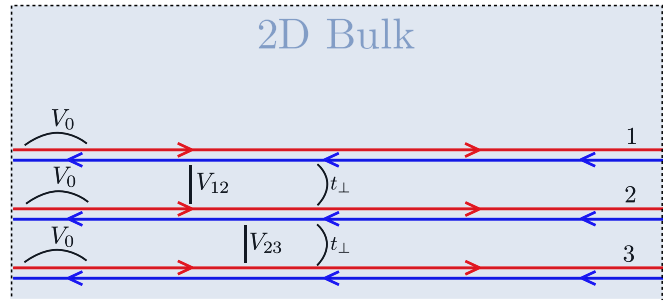

FIG. 1. Three helical modes on the edge of a two-dimensional TI. We label the different channels by 1,2, and 3 and the different interaction strengths V_0, V_{12}, V_{23} as depicted. Tunneling amplitude between modes $1-2$ and $2-3$ is denoted by $t_{\perp}$. Tunneling between 1 and 3 is assumed to be negligible.

In the band basis that corresponds to

$$\psi^{\eta}_{k,1(3)} = \frac{c^{\eta}_{k,1} \pm \sqrt{2} c^{\eta}_{k,2} + c^{\eta}_{k,3}}{2}, \quad \psi^{\eta}_{k,2} = \frac{c^{\eta}_{k,1} - c^{\eta}_{k,3}}{\sqrt{2}}, \tag{2}$$

the single-particle Hamiltonian is diagonal and the energy dispersion relations are given by

$$E^{a}_{\eta} = \eta v_F k + \lambda_a t_{\perp}, \tag{3}$$

with $\lambda_a = (-1, 0, 1)$. These energy dispersion relations are depicted in Fig. 2.

Note that the single-particle Hamiltonian is invariant under the symmetry of interchanging modes $1 \leftrightarrow 3$. This symmetry is not expected to hold in general, and we break it explicitly in the general model of Appendix A.

B. Interactions

A generic interaction between the three different helical modes is described by the following lattice Hamiltonian:

$$H_{\text{int}} = \sum_{i,a} V_0 n_{i,a} n_{i+1,a} + 2 \sum_{i} (V_{12} n_{i,1} n_{i,2} + V_{23} n_{i,2} n_{i,3}), \tag{4}$$

where the density at each site i and channel a is $n_{i,a} = \sum_{\sigma} (c^{\sigma}_{i,a})^{\dagger} c^{\sigma}_{i,a}$. The interaction parameter V_0 denotes the intramode interaction, while V_{ab} denotes the interaction between modes a and b. For simplicity of the exposition, here we do not consider the interaction between modes 1 and 3, although such interaction is considered in Appendix A. In the basis that diagonalizes the Hamiltonian, the density for the band a and helicity η corresponds to $\rho^{\eta}_{i,a} = (\psi^{\eta}_{i,a})^{\dagger} \psi^{\eta}_{i,a}$. Summing over the helicities we have the total density per band $\rho_{i,a} = (\psi^{+}_{i,a})^{\dagger} \psi^{+}_{i,a} + (\psi^{-}_{i,a})^{\dagger} \psi^{-}_{i,a}$. The total density on each site is $\rho_i = \sum_a \rho_{i,a}$.

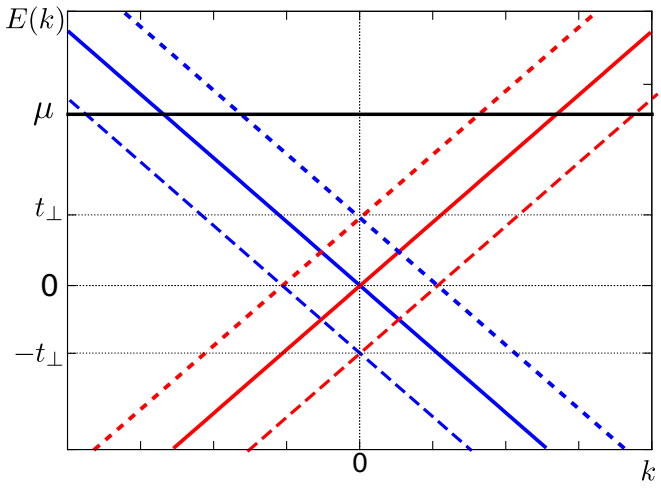

FIG. 2. Single-particle spectrum for the different modes in the band basis. We consider a linear approximation to the energy spectrum. Solid lines denote the two chiralities of mode 2 in the band basis, while the (short) dashed lines indicate the two chiralities of the mode (1) 3 in the band basis. Note that the crossing points around $k \sim 0$ are protected by TR symmetry so a gap does not open. All the other crossings are not protected, and in principle, energy gaps can be opened. We assume that the chemical potential μ is such that the Fermi energy does not intersect any crossing point (represented here by the black horizontal line). This implies that the low-energy physics is captured by three helical modes, where our discussion of the main text applies.

In the low-energy, long-wavelength limit we can introduce a continuous description of the modes and expand the fields around the Fermi points (here $x = ia_0$, with a_0 the lattice spacing)

$$\frac{\psi^{\eta}_{i,a}}{\sqrt{a_0}} = \psi_{a,\eta}(x), \tag{5}$$

together with the slowly varying fields $\psi_{a,+}(x) = R_a(x)e^{ik^a_F x}$ and $\psi_{a,-}(x) = L_a(x)e^{-ik^a_F x}$. Fixing the chemical potential away from the band crossings and considering $t_\perp \neq 0$, the Fermi momenta become $k^a_F = \frac{\mu+\lambda_a t_\perp}{v_F}$. In the continuous description, the noninteracting part of the Hamiltonian is given by

$$H_0 = iv_F \sum_a \int dx (R^\dagger_a \partial_x R_a - L^\dagger_a \partial_x L_a). \tag{6}$$

Collecting processes that conserve momentum (i.e., do not have oscillations with k_F), the interaction sector of the Hamiltonian becomes (omitting the space dependence of the densities) $H_{\rm int} = H_{\rho\rho} + H_{\rm nl}$, with

$$H_{\rho\rho} = \int dx \Big(\tilde{V}_0 \rho^2 + g(\rho_1+\rho_3)^2 + g'\rho_2^2 + \tilde{g}\sum_\eta \rho^\eta_1 \rho^\eta_3 + 4g \sum_\eta \rho^\eta_2 (\rho^\eta_1 + \rho^\eta_3) \Big), \tag{7}$$

containing the forward-scattering interaction terms, and

$$H_{\rm nl} = \tilde{g}\int dx (R^\dagger_1 R_3 L^\dagger_1 L_3 + L^\dagger_3 L_1 R^\dagger_3 R_1) + 4g \int dx (L^\dagger_1 L_2 R^\dagger_2 R_3 + L^\dagger_2 L_3 R^\dagger_1 R_2 + \text{H.c.}) + 4g \int dx (L^\dagger_2 L_3 R^\dagger_2 R_3 + L^\dagger_1 L_2 R^\dagger_1 R_2 + \text{H.c.}), \tag{8}$$

containing the extra interaction terms. Here $\tilde{V}_0 = \frac{a_0}{4}(V_0 + V_{12} + V_{23})$ and

$$g = \frac{V_0 a_0}{8}, \quad g' = \frac{(V_0 - V_{23} - V_{12})a_0}{4}, \quad \tilde{g} = 2(g+g'). \tag{9}$$

Note that the full Hamiltonian is invariant under the operation of permuting the modes $1 \leftrightarrow 3$ and the interaction strengths $V_{12} \leftrightarrow V_{23}$.

Taking $g = 0$ (or $g_2 = 0$ in the general model of Appendix A), the three helical model reduces to the two helical system studied in Ref. [24], plus a forward-scattering interaction with the antisymmetric band mode ψ^η_2.

In the limit of zero tunneling $t_\perp = 0$, there is another operator that conserves momentum, given by

$$\mathcal{O}_{t_\perp=0} = \tilde{g}\int dx R^\dagger_1 L_1 L^\dagger_3 R_3. \tag{10}$$

The presence of this operator, together with the other operator involving just modes 1 and 3 [first line of Eq. (8)], modifies the low-energy behavior of the model, preventing the opening of a gap between modes 1 and 3, as can be observed in the case of two helical modes [24]. This result is in line with the intuition that independent helical modes interacting through their densities, away from commensurate filling, are not gapped by interactions.

III. BOSONIZATION ANALYSIS

We represent the slow part of the fermionic operators as vertex operators of a bosonic field, as is standard in bosonization [34,35], by $R_a(x) = \frac{\kappa_a}{\sqrt{2\pi a_0}} e^{i\sqrt{4\pi}\phi_{R,a}(x)}$ and $L_a(x) = \frac{\kappa_a}{\sqrt{2\pi a_0}} e^{-i\sqrt{4\pi}\phi_{L,a}(x)}$. Here κ_a is a Klein factor satisfying $\{\kappa_a, \kappa_b\} = 2\delta_{ab}$. The bosonic fields satisfy the equal time commutation relations $[\phi_{\eta,a}(x), \phi_{\eta',b}(y)] = \frac{i}{4}\eta\delta_{ab}\delta_{\eta\eta'}\text{sgn}(x-y)$, with $\eta = (+,-) = (R,L)$. Using these conventions, the bosonized form of the density in band a and with helicity η is $\rho^\eta_a = \frac{1}{\sqrt{2\pi}}\partial_x \phi_{\eta,a}$.

It is useful to define the following fields:

$$\tilde{\phi}_{\eta,c}(x) = \sum_{a=1}^{3} \frac{\phi_{\eta,a}(x)}{\sqrt{3}}, \quad \tilde{\phi}_{\eta,\mu}(x) = \sum_{a=1}^{3} d^\mu_a \phi_{\eta,a}(x), \tag{11}$$

together with the inverse relation $\phi_{\eta,a}(x) = \frac{1}{\sqrt{3}}\tilde{\phi}_{c\eta}(x) + \sum_\mu d^\mu_a \tilde{\phi}_{\eta,\mu}(x)$. The vectors $\boldsymbol{d}$ correspond to the three vertices of an equilateral triangle, see Fig. 3, and are explicitly given by

$$\boldsymbol{d}_1 = \begin{pmatrix} \frac{1}{\sqrt{2}} \\ \frac{1}{\sqrt{6}} \end{pmatrix}, \quad \boldsymbol{d}_2 = \begin{pmatrix} 0 \\ -\frac{2}{\sqrt{6}} \end{pmatrix}, \quad \boldsymbol{d}_3 = \begin{pmatrix} -\frac{1}{\sqrt{2}} \\ \frac{1}{\sqrt{6}} \end{pmatrix}. \tag{12}$$

They satisfy $\boldsymbol{d}_a \cdot \boldsymbol{d}_b = \delta_{ab} - \frac{1}{3}$.

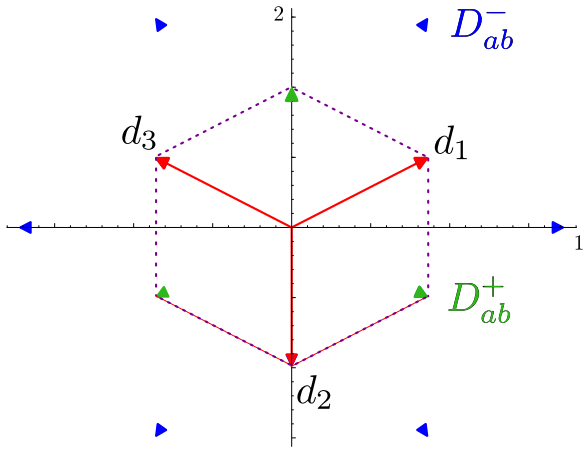

FIG. 3. Vectors defining the neutral fields and the different order parameters. The vectors of neutral fields form an equilateral triangle (red arrows). The horizontal (vertical) axis corresponds to the direction of the neutral field $\tilde{\phi}_{\eta,1}(\tilde{\phi}_{\eta,2})$. These arrows generate a lattice of possible processes. The lattice points corresponding to $\boldsymbol{D}^{+(-)}_{ab} = \boldsymbol{d}_a + (-)\boldsymbol{d}_b$ are depicted in green (blue). Note that a process containing any combination of $\boldsymbol{D}^{-}_{ab} \cdot \tilde{\boldsymbol{\theta}}$ always contains the field $\tilde{\theta}_1$. This makes the superconducting order parameters short ranged.

We introduce the nonchiral fields $\tilde{\varphi}_a = \tilde{\phi}_{R,a} - \tilde{\phi}_{L,a}$ and $\tilde{\theta}_a = \tilde{\phi}_{R,a} + \tilde{\phi}_{L,a}$, with $a = c, 1, 2$. The only nonvanishing commutation relations in this basis are $[\partial_x\tilde{\varphi}_a(x), \tilde{\theta}_b(y)] = i\delta_{ab}\delta(x-y)$. For future reference, we also introduce the basis for neutral fields $\tilde{\boldsymbol{\varphi}} = (\tilde{\varphi}_1, \tilde{\varphi}_2)$ and $\tilde{\boldsymbol{\theta}} = (\tilde{\theta}_1, \tilde{\theta}_2)$.

In order to identify the total charge mode we perform a global U(1) transformation on the original fermionic fields $\psi_{a,\eta}(x) \to \psi_{a,\eta}(x)e^{i\Theta}$, which amounts to a shift in the bosonic fields as $\phi_{\eta,a} \to \phi_{\eta,a} + \frac{\Theta}{\sqrt{4\pi}}$. The fields defined in (11) transform as $\tilde{\phi}_{\eta,c} \to \tilde{\phi}_{\eta,c} + \sqrt{\frac{3}{4\pi}}\Theta$ and $\tilde{\phi}_{\eta,\mu} \to \tilde{\phi}_{\eta,\mu}$. This implies that the fields $\tilde{\theta}_c, \tilde{\varphi}_c$ describe the total charge mode and its conjugate field, while the modes $\tilde{\theta}_{1,2}$ and their conjugates are neutral with respect to the total U(1) charge.

The Hamiltonian of the system $H = H_0 + H_{\rho\rho} + H_{\rm nl}$ in the bosonized variables splits into $H = H_c + H_1 + H_2 + H_{\rm mix}$, where the total charge sector H_c is

$$H_c = \frac{v_c}{2}\int dx\left(K_c(\partial_x\tilde{\varphi}_c)^2 + \frac{1}{K_c}(\partial_x\tilde{\theta}_c)^2\right), \tag{13}$$

while the Hamiltonians for the neutral sectors H_1 and H_2 are

$$H_1 = \frac{v_1}{2}\int dx((\partial_x\tilde{\varphi}_1)^2 + (\partial_x\tilde{\theta}_1)^2) + \frac{g+g'}{(\pi a_0)^2}\int dx\cos(\sqrt{8\pi}\tilde{\varphi}_1), \quad \text{and} \tag{14}$$

$$H_2 = \frac{v_2}{2}\int dx\left(K_2(\partial_x\tilde{\varphi}_2)^2 + \frac{1}{K_2}(\partial_x\tilde{\theta}_2)^2\right) + \frac{4g}{(\pi a_0)^2} \times \int dx(\cos(\sqrt{6\pi}\tilde{\varphi}_2) + \cos(\sqrt{6\pi}\tilde{\theta}_2))\cos(\sqrt{2\pi}\tilde{\varphi}_1), \tag{15}$$

respectively. The renormalized velocities and Luttinger parameters of these modes satisfy $v_1 = v_F - \frac{g+g'}{2\pi}$:

$$v_2K_2 = v_1 + \frac{2(g'-g)}{3\pi}, \quad v_2K_2^{-1} = v_1 + \frac{4g'}{3\pi},$$
$$v_cK_c = v_F + \frac{g'+5g}{3\pi}, \quad v_cK_c^{-1} = v_F + \frac{2g'}{3\pi} + \frac{3(g+\tilde{V}_0)}{\pi}. \tag{16}$$

Note that the mode $\tilde{\theta}_1$ sees its velocity renormalized, but its Luttinger parameter stays unity as a consequence of TR symmetry and the fact that the microscopic degrees of freedom are helical. This implies that at all orders in the interaction parameters the scaling dimension $\Delta_1^{\varphi}(\alpha) \equiv \Delta[\cos(\sqrt{2\alpha\pi}\tilde{\varphi}_1)] = \alpha$. The remaining part of the Hamiltonian is

$$H_{\rm mix} = \frac{\sqrt{2}}{6\pi}\int dx[(g'-g)\partial_x\tilde{\varphi}_c\partial_x\tilde{\varphi}_2 + (3g-g')\partial_x\tilde{\theta}_c\partial_x\tilde{\theta}_2]. \tag{17}$$

It couples the total charge mode and the second neutral sector. This term is strictly marginal and does not influence the physics in any of the gapped phases, as the field $\tilde{\varphi}_2$ ($\tilde{\theta}_2$) is locked by the renormalization of the cosine terms in the ET (TRSB) phase. To first order in the interaction parameters the scaling dimensions of the cosine terms are

$$\Delta_2^{\varphi} \equiv \Delta[\cos(\sqrt{6\pi}\tilde{\varphi}_2)] = \frac{3}{2} + \frac{g+g'}{\pi v_F}, \tag{18}$$

$$\Delta_2^{\theta} \equiv \Delta[\cos(\sqrt{6\pi}\tilde{\theta}_2)] = \frac{3}{2} - \frac{g+g'}{\pi v_F}. \tag{19}$$

The value of the scaling dimensions determines the fate of the cosine operators under the renormalization group (RG). We now consider two limiting cases of purely attractive and purely repulsive interaction. We start with the former, assuming $g = g'$ [$V_0 = 2(V_{12} + V_{23})$] for simplicity.

A. Attractive interactions

In this case $g < 0$ and $\Delta_2^{\theta} > \Delta_2^{\varphi}$, so the cosine operator $\cos(\sqrt{6\pi}\tilde{\varphi}_2)$ grows faster than $\cos(\sqrt{6\pi}\tilde{\theta}_2)$ under renormalization. Keeping the maximal set of commuting cosine operators with the smallest scaling dimensions, the model becomes a marginal deformation of the SU(3) Gross-Neveu model [36] and is given by

$$H = H_c + H_{\rm SU(3)} + \frac{\sqrt{2}g}{3\pi}\int dx\partial_x\tilde{\theta}_c\partial_x\tilde{\theta}_2 + +, \frac{4g}{3\pi}\int dx(\partial_x\tilde{\theta}_2)^2 + \frac{2g}{\pi}\sum_a\int dx(\partial_x\tilde{\varphi}_a)^2. \tag{20}$$

Here the SU(3) symmetric sector is described by

$$H_{\rm SU(3)} = \sum_{a=1}^{2}\int dx\frac{v_1}{2}((\partial_x\tilde{\varphi}_a)^2 + (\partial_x\tilde{\theta}_a)^2) - \frac{2g}{\pi}\sum_a\int dx(\partial_x\tilde{\varphi}_a)^2 + \frac{2g}{(\pi a)^2}\int dx\cos(\sqrt{8\pi}\tilde{\varphi}_1) + \frac{4g}{(\pi a)^2}\int dx\cos(\sqrt{6\pi}\tilde{\varphi}_2)\cos(\sqrt{2\pi}\tilde{\varphi}_1). \tag{21}$$

As the prefactors of the cosines flow to strong coupling under RG, the energy of this Hamiltonian is minimized for specific constant values of the field $\tilde{\varphi}_1, \tilde{\varphi}_2$. This locking opens a gap in the spectrum of the neutral sector. In general, the sign of the amplitude in front of the cosine terms determines the structure of the ground state. In the case that we are considering here, this amplitude is negative, so the fields $(\tilde{\varphi}_1, \tilde{\varphi}_2)$ lock to the values $(0, 0)$. As we will show below, this phase is topological due to the pinning of the neutral field $\tilde{\varphi}_2$. The topological nature of this phase is manifested in two ways: (a) in the stability of a metallic phase against weak disorder, and (b) in domain wall configurations that host localized fractionalized zero modes. In this phase, TR symmetry is not broken.

Although for the "simplified" model discussed above, this phase appears only for attractive interactions, for a more generic case (see Fig. 5) the topological phase can emerge for purely repulsive interactions as well.

B. Repulsive interactions

In this regime $g > 0$ and the scaling dimensions satisfy $\Delta_2^\theta < \Delta_2^\varphi$, making the cosine operator $\cos(\sqrt{6\pi}\tilde{\theta}_2)$ the most relevant operator in RG sense. Keeping the largest set of cosine operators that commute with $\tilde{\theta}_2$, the Hamiltonian becomes

$$H = H_c + \widetilde{H}_{\mathrm{SU}(3)} + \frac{\sqrt{2}g}{3\pi}\int dx \partial_x\tilde{\theta}_c\partial_x\tilde{\theta}_2 + \frac{10g}{3\pi}\int dx(\partial_x\tilde{\theta}_2)^2 + \frac{2g}{\pi}\int dx(\partial_x\tilde{\varphi}_1)^2. \quad (22)$$

The Hamiltonian $\widetilde{H}_{\mathrm{SU}(3)}$ can be obtained from (21) by the chiral transformation that interchanges $\tilde{\varphi}_2 \leftrightarrow \tilde{\theta}_2$.

The cosine operator $\cos(\sqrt{6\pi}\tilde{\theta}_2)$ grows faster under renormalization, opening a gap and locking the value of the field $\tilde{\theta}_2$. The field values $(\tilde{\varphi}_1^*, \tilde{\theta}_2^*)$ that minimize the energy are given semiclassically by the solutions of the equations

$$\cos(\sqrt{6\pi}\tilde{\theta}_2^*) + 2\cos(\sqrt{2\pi}\tilde{\varphi}_1^*) = 0,$$
$$\sin(\sqrt{6\pi}\tilde{\theta}_2^*)\cos(\sqrt{2\pi}\tilde{\varphi}_1^*) = 0,$$

which for a repulsive interaction in the special point $g = g' > 0$ are given by $(\sqrt{2\pi}\tilde{\varphi}_1^*, \sqrt{6\pi}\tilde{\theta}_2^*) = (\pm\frac{2\pi}{3}, 0)$, or by $(\sqrt{2\pi}\tilde{\varphi}_1^*, \sqrt{6\pi}\tilde{\theta}_2^*) = (\pm\frac{\pi}{3}, \pi)$ with a double-degenerate vacua. The dominant order parameters in this phase are odd under TR transformations, indicating the onset of spontaneous breaking of TR in this phase. This phase is not topologically protected, as disorder or interaction can gap the charge mode.

C. Generic conditions for the appearance of the different massive phases

Considering a generic model (see Appendix A) where we allow for general tunneling amplitudes t_L between modes 1 and 2 and t_R between modes 2 and 3, we find that both phases can be reached for sufficiently attractive or repulsive interactions, depending on the particular intra- and interchannel interaction strengths. For a simple case of $V_{12} = V_{23} \equiv V_\perp$ and $t_R = t_L$, the phase diagram is given by Fig. 4. In the more general case of arbitrary tunneling amplitudes t_L and t_R and intrachannel interaction larger than interchannel interaction $V_\perp < V_0$, we find that it is possible to reach the ET phase with purely repulsive interactions if the intermode tunneling is close to the symmetric case $t_L = t_R$ and the intermode interaction $V_\perp$ is comparable with the intermode interaction strength $V_\perp \sim 3/4V_0$ (see also Fig. 5).

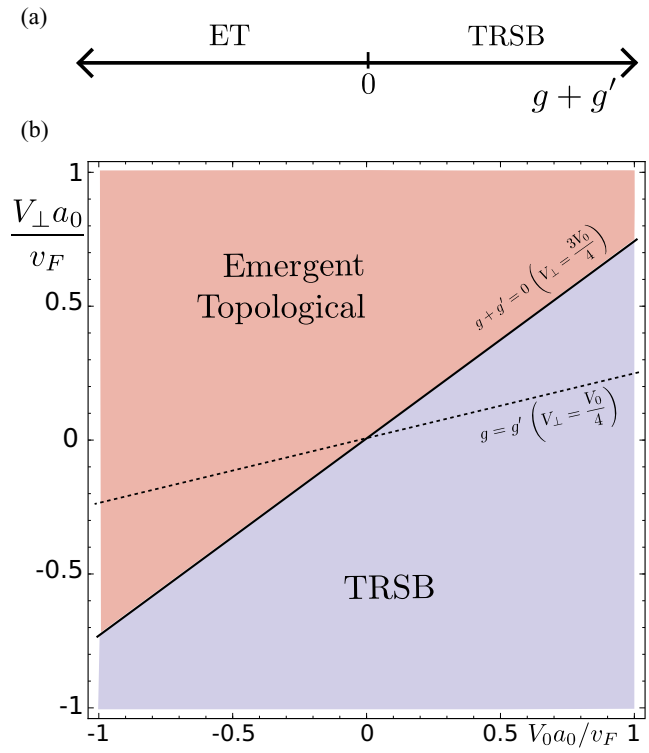

FIG. 4. (a) Different phases as a function of the parameter $g + g'$, defined in (9). [See also Eq. (A10) in Appendix.] (b) The phase diagram for the model of Sec. II as a function of the intramode (V_0) and intermode ($V_\perp$) interactions. Here we assume the same interaction strength between channels ($V_{12} = V_{23} = V_\perp$). The transition line between the TRSB and ET phase happens at $g + g' = 0$. The diagonal dashed line corresponds to the simple limit $g = g'$, considered in Sec. III.

Below we characterize the ET and TRSB phases in terms of local order parameters.

IV. CHARACTERIZATION OF THE PHASES

A. Two-particle normal order parameters

The usual order parameters involving two-particle number-conserving processes are given by $\mathcal{O}_\alpha^{\mathrm{ord}} = \sum_{ab}(\psi_{a,L}^\dagger \lambda_{ab}^{(\alpha)}\psi_{b,R} + \psi_{b,R}^\dagger \lambda_{ab}^{(\alpha)*}\psi_{a,L})$, where $\boldsymbol{\lambda}^{(\alpha)}$ are the Gell-Mann matrices [37]. These order parameters can be separated as time-reversal even or time-reversal odd by $\mathcal{T}\mathcal{O}_{\alpha,\pm}^{\mathrm{ord}}\mathcal{T}^{-1} = \pm\mathcal{O}_{\alpha,\pm}^{\mathrm{ord}}$. For the even operators we have that $\lambda_{ab}^{(\alpha)} = -\lambda_{ba}^{(\alpha)}$, while for the odd operators $\lambda_{ab}^{(\alpha)} = \lambda_{ba}^{(\alpha)}$. The 3×3 antisymmetric Hermitian matrices can be generated by linear combinations of generators of the SU(3) Lie algebra $\boldsymbol{\lambda}^{(\alpha)}$ in the fundamental representation (with $\alpha \in \alpha_{\mathrm{even}} = \{2, 5, 7\}$) while the symmetric Hermitian 3×3 matrices are generated by linear combinations of $\boldsymbol{\lambda}^{(\alpha)}$, with

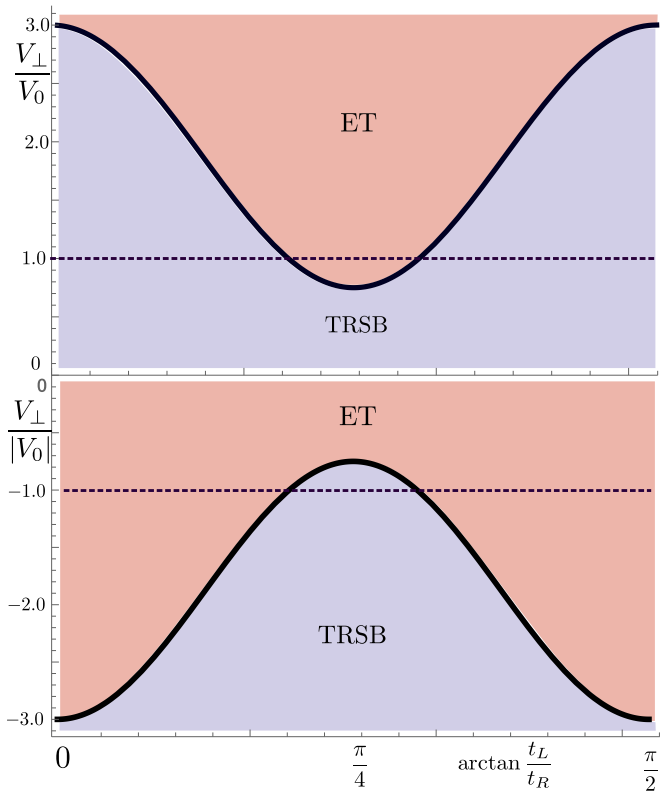

FIG. 5. In a more general model that includes different tunneling amplitudes between modes 1-2 (t_L) and 2-3 (t_R) the phase diagram depends on the specific value of the ratio $\frac{t_L}{t_R}$. Assuming the situation $V_{12} = V_{23} = V_\perp < V_0$, the ET phase can be reached for specific repulsive interactions (top panel $V_0 > 0$) around the symmetric point $t_R \sim t_L$ and generic attractive interactions (lower panel). The TRSB phase can be reached with generic repulsive interactions (top panel) and specific attractive interactions (lower panel) around the region of symmetric tunneling.

$\alpha \in \alpha_{\rm odd} = \{0, 1, 3, 4, 6, 8\}$, where $\boldsymbol{\lambda}^{(0)}$ is the 3×3 identity matrix.

The odd (even) operators under TR are given by $\mathcal{O}^{\rm ord}_\alpha$, with $\alpha \in \alpha_{\rm odd}$ ($\alpha_{\rm even}$). The even operators describe the processes of electron hopping that are TR invariant, i.e., terms that can be added to the Hamiltonian. The operators that are odd under TR symmetry cannot be included into the Hamiltonian without explicitly breaking TR symmetry. Using bosonization and omitting Fermi momentum contributions, these operators become, in the basis $\tilde{\boldsymbol{\varphi}}, \tilde{\boldsymbol{\theta}}$,

$$\mathcal{O}^{\rm ord}_\alpha = \sum_{ab} \tilde{\lambda}^{(\alpha)}_{ab} \cos\left[\sqrt{\pi}\left(\boldsymbol{D}^+_{ab}\cdot\tilde{\boldsymbol{\theta}} + \frac{2\tilde{\theta}_c}{\sqrt{3}}\right)\right] e^{i\sqrt{\pi}\boldsymbol{D}^-_{ba}\cdot\tilde{\boldsymbol{\varphi}}}, \quad (23)$$

where $\boldsymbol{D}^\pm_{ab} = \boldsymbol{d}_a \pm \boldsymbol{d}_b$ (see also Fig. 3). Here we have also incorporated the Klein factors κ_a in the definition $\tilde{\lambda}^{(\alpha)}_{ab} = \lambda^{(\alpha)}_{ab}\bar{\kappa}_a\kappa_b$. In the TRSB phase (where $\tilde{\theta}_2$ is pinned) we observe that the order parameters $\mathcal{O}^{\rm ord}_4$, $\mathcal{O}^{\rm ord}_5$ and the combination $\mathcal{O}_{II} \equiv \frac{i}{2}(\psi^\dagger_{2,L}\psi_{2,R} - \psi^\dagger_{2,R}\psi_{2,L})$ become quasi-long-ranged ordered (QLRO). The correlation function between any of these three order parameters is $\langle \mathcal{O}^{\rm ord}_\alpha(x)\mathcal{O}^{\rm ord}_\beta(0)\rangle \sim |x|^{\frac{-2K_c}{3}}$ for $\alpha, \beta = (4, 5, II)$ and with a wave vector $2k^2_F$. The correlation functions between all other two-particle normal order parameters decay exponentially. On the other hand, in the ET phase (where the bosonic field $\tilde{\varphi}_2$ is pinned) all normal order parameters do not exhibit QLRO and decay exponentially with distance.

B. Superconducting order parameters

We can also study the superconducting order parameters given by $\mathcal{S}^{\rm ord}_\alpha = \sum_{ab}(\psi^\dagger_{a,L}\lambda^{(\alpha)}_{ab}\psi^\dagger_{b,R} + \psi_{b,R}\lambda^{(\alpha)*}_{ab}\psi_{a,L})$. These operators do not develop QLRO in any phase, as they always contain the field $\tilde{\theta}_1$, dual to $\tilde{\varphi}_1$, which is locked in both phases (see also Fig. 3). Correlation functions of these order parameters decay exponentially with distance in the ground state. This implies that there is no superconducting order in any of the phases.

C. Trionic order parameters

As we have discussed, in both ET and TRSB phases the low-energy Hamiltonian of the model corresponds to an adiabatic deformation of an SU(3) Gross-Neveu model. Based on this structure, we can use the fundamental representation of SU(3) in terms of fermions to construct an order parameter. Starting from the complete antisymmetric Young tableaux corresponding to $\begin{smallmatrix}\square\\\square\end{smallmatrix} = c^\dagger_1 c^\dagger_2 c^\dagger_3$, we define (in the band basis) the order parameter

$$\mathcal{T}_I = \psi^\dagger_1\psi^\dagger_2\psi^\dagger_3 + \text{H.c.}, \quad (24)$$

with $\psi_a = \psi^+_a + \psi^-_a$. In the TRSB phase the order parameter $\mathcal{T}_I$ acquires QLRO, with the correlation function satisfying

$$\langle \mathcal{T}_I(x)\mathcal{T}_I(0)\rangle \sim \frac{\sin(k_3 x)}{|x|^{\frac{1}{2}(\frac{3}{K_c}+\frac{K_c}{3})}}, \quad (25)$$

with wave vector $k^3_F - k^1_F + k^2_F$. This trionic order parameter is dominant for strong attractive interactions such that $K_c > \sqrt{3} \sim 1.7$. We recall that for the special point $g = g'$ in the model (7)–(8), the trionic order parameter is never more dominant than the two-particle operator $\mathcal{O}^{\rm ord}_{4,5,II}$ of Eq. (23). In the general model of Appendix A, we see that there is a region where the trionic order parameter is dominant for strong enough interaction.

In contrast, in the ET phase the conjugate field $\tilde{\varphi}_2$ is locked. This implies that all two-particle order parameters have exponentially decaying expectation values. In particular, this indicates that the backscattering processes generated by the existence of impurities do not affect the conduction properties in this phase, at least at leading order on the impurity strength.

As there are no two-particle order parameters that dominate in the ET phase, we look for three-particle order parameters. We find that the operator

$$\mathcal{T}_{II} = \frac{\psi_1\psi^\dagger_2\psi^\dagger_3 + \psi^\dagger_1\psi_2\psi^\dagger_3 + \psi^\dagger_1\psi^\dagger_2\psi_3}{\sqrt{3}} + \text{H.c.} \quad (26)$$

has a dominant correlation function (discarding the purely right/left contributions $R^\dagger_1 R_2 R_3$, etc.),

$$\langle \mathcal{T}_{II}(x)\mathcal{T}_{II}(0)\rangle \sim \frac{\sin(3k_2 x)}{|x|^{\frac{1}{2}(3K_c+\frac{1}{3K_c})}}. \quad (27)$$

This phase is protected against single-particle disorder, and its charge mode cannot be gapped by either two or four fermion terms, regardless of their microscopic origin. This is a feature of the ET phase. In the following section we discuss on general grounds the topological properties of the TRSB and ET phases.

V. THE STABILITY OF TOPOLOGICAL PHASES AGAINST INTERACTIONS

So far we have analyzed the model of three interacting helical modes, having in mind a microscopic realization. Now we shift the point of view to a more general perspective. Here we ask, Once the TRSB or ET phases are fully developed, *is it possible to gap their charge mode, without explicitly breaking TR symmetry?* We ask this question irrespective of any microscopic realization. For any given model, some of the terms discussed below will not appear due to momentum conservation or incommensurability. Anyway, they are allowed by the TR symmetry, and we consider them.

In the case of two-fermion operators, we have already seen that terms exist that can backscatter the helical modes in the TRSB phase and do not decay exponentially. These terms are already present in the noninteracting limit and are responsible for reducing the classification of two-dimensional TR-invariant systems from $\mathbb{Z}$ to $\mathbb{Z}_2$. For temperatures comparable with the largest gap in the neutral sector, we can estimate their effect by using the noninteracting Landauer formula [38], replacing the noninteracting parameters with the renormalized ones, given by the flow of the backscattering amplitudes due to the interactions. We do this explicitly in Sec. VII. Clearly, for lower temperatures, where the gaps in the neutral sector are the largest energy scale, extended backscattering terms **can** gap the charge mode in the TRSB phase, so this phase is **not** topologically protected. On the other hand, in the ET phase, all two-fermion operators decay exponentially, so they cannot localize the charge mode.

A general operator allowed by TR symmetry in a system of three helical edges corresponds to a polynomial in the operators

$$\mathcal{O}^{\theta}_{\boldsymbol{n},\delta} = \cos[\sqrt{4\pi}(\boldsymbol{n}\cdot\boldsymbol{\theta}) + \delta], \quad \mathcal{O}^{\varphi}_{\boldsymbol{n}} = \exp(i\sqrt{4\pi}\boldsymbol{n}\cdot\boldsymbol{\varphi}), \tag{28}$$

with $\theta_a(\varphi_a) = \phi_{R,a} + (-)\phi_{L,a}$. Here the parameter δ is an arbitrary real number and the vector $\boldsymbol{n}$ has integer components. Due to TR symmetry, it satisfies $\sum_a n_a = 0 \bmod 2$. In the basis of charge and neutral modes, these operators respectively become

$$\mathcal{O}^{\theta}_{\boldsymbol{n},\delta} = \cos\left[\sqrt{4\pi}\left(\frac{2p\tilde{\theta}_c}{\sqrt{3}} + \sum_a n_a \boldsymbol{d}_a\cdot\tilde{\boldsymbol{\theta}}\right) + \delta\right], \tag{29}$$

$$\mathcal{O}^{\varphi}_{\boldsymbol{n}} = \exp\left[i\sqrt{4\pi}\left(\frac{2p\tilde{\varphi}_c}{\sqrt{3}} + \sum_a n_a \boldsymbol{d}_a\cdot\tilde{\boldsymbol{\varphi}}\right)\right], \tag{30}$$

where we have used $\sum_a n_a = 2p$, $p\in\mathbb{Z}$. For example, the superconducting operators $\mathcal{S}^{\mathrm{ord}}_{(\alpha_{\mathrm{odd}})}$ defined in Sec. IV B can be written in terms of these general operators as $\mathcal{S}^{\mathrm{ord}}_{(\alpha_{\mathrm{odd}})} \propto \sum_{ab}\lambda^{(\alpha_{\mathrm{odd}})}_{ab}\mathcal{O}^{\theta}_{\boldsymbol{n}^-_{ba},0}\mathcal{O}^{\varphi}_{\boldsymbol{n}^+_{ba}}$, where we have introduced the vectors $\boldsymbol{n}^{\pm}_{ab}$ defined componentwise as $(\boldsymbol{n}^{\pm}_{ab})_r \equiv \delta_{br} \pm \delta_{ar}$. The other superconducting operators can be written similarly. As we mentioned earlier, all of these operators have some contribution from $(\boldsymbol{d}_b - \boldsymbol{d}_a)\cdot\tilde{\boldsymbol{\theta}}$, which always has a component proportional to $\tilde{\theta}_1$ (see Fig. 3), rendering the superconducting operators irrelevant in both gapped phases.

In the TRSB phase, where the pair $\tilde{\varphi}_1, \tilde{\theta}_2$ is locked, it is easy to find an operator that locks the charge mode $\tilde{\theta}_c$. A solution (of the infinitely many) is given by $n_1 = n_3 = 1$ and $n_2 = 0$, which corresponds to the operator

$$\mathcal{O}^{\theta}_{(1,0,1)} = R^{\dagger}_1 L_1 R^{\dagger}_3 L_3 + \mathrm{H.c.} \tag{31}$$

In the ET phase, on the other hand, the locked fields are $\tilde{\varphi}_1, \tilde{\varphi}_2$. In this phase we can only use the operator $\mathcal{O}^{\varphi}_{\boldsymbol{n}}$ to lock the (conjugate) charge field, as this is the only operator that commutes with the operators that open the neutral gaps. The operator $\mathcal{O}^{\varphi}_{\boldsymbol{n}}$ does not conserve the overall charge (because to lock $\tilde{\varphi}_c$ it has to have $p \neq 0$). We have encountered operators of this kind in the discussion of trionic order parameters $\mathcal{T}_{II}$ in the ET phase. Although this operator survives in the ET phase, it cannot be used by itself to lock the charge mode, as it is fermionic and cannot appear as a term in the Hamiltonian. A valid term that can be included in the Hamiltonian and could serve to lock the charge mode in the ET phase is $\mathcal{T}_{II}(x)\mathcal{T}_{II}(x+a)$. These results can be summarized as

Q: *Is it possible to gap the charge mode in a given phase, without explicitly breaking TR symmetry?*

A: In the TRSB phase, it is possible, so this phase is not topologically protected in the presence of interactions. In the ET phase, on the other hand, it is **not** possible to gap the charge mode without also breaking particle number conservation, so this phase is protected by TR symmetry and particle number conservation. This general analysis implies in particular that the different phases of the microscopic model of three coupled helical wires discussed above are stable under any perturbation that does not violate TR symmetry. This suggests that the model at hand is a representative example for many systems with the same topological properties. It is important to note that the only way of gapping the charge mode in the ET phase is through locking the $\tilde{\varphi}_c$, which breaks TR symmetry spontaneously if the locking value is different from zero or π, as this field is odd under TR and compact.

A. Spontaneous breaking of TR in the trivial phase

As its name indicates, the TRSB phase spontaneously breaks the TR symmetry in the ground state. One way of seeing this is by considering the expectation value of operators that describe backscattering between Kramers pairs. These are given by the TR-odd Hermitian operators

$$\mathcal{O}_{\mathrm{Kr},a} = \frac{1}{2}\sum_{\eta\eta'}\psi^{\dagger}_{a\eta}(x)(\sigma_y)_{\eta\eta'}\psi_{a\eta'}(x), \tag{32}$$

which in the bosonized form becomes

$$\mathcal{O}_{\mathrm{Kr},a} \sim \sin\left[2k_{F,a}x + \sqrt{4\pi}\left(\frac{\tilde{\theta}_c}{\sqrt{3}} + \boldsymbol{d}_a\cdot\tilde{\boldsymbol{\theta}}\right)\right]. \tag{33}$$

The order parameter $\mathcal{O}_{\mathrm{Kr},2}$ acquires a constant contribution when the charge mode is gapped, which is possible only in the phase where $\tilde{\theta}_2$ is locked. The order parameters $\mathcal{O}_{\mathrm{Kr},1}$

and $\mathcal{O}_{\mathrm{Kr},3}$ decay exponentially in the TRSB phase. In particular, this occurs for the microscopic model of Sec. II at $\mu = 0$ (which corresponds to a commensurability condition that allows single-particle Umklapp scattering), where the operator $\mathcal{O}^{\theta}_{(1,0,1)}$ conserves momentum and locks the charge mode. The presence of a constant order parameter that is odd under TR symmetry indicates the spontaneous breaking of TR symmetry in the ground state.

We note that due to the coupling in the charge mode, this order parameter has QLRO whenever the charge mode is gapless. We stress that this consideration is based purely on general grounds and is not associated with a particular underlying microscopic model. The ET phase, on the other hand, does not break TR spontaneously.

B. Relation with one and two helical modes

We observe that the topological protection of the noninteracting system can be absent once we include interactions. It is illustrative to consider some simple limits where the breaking of noninteracting topological protection is clearly demonstrated. Taking $g = 0$ in our microscopic model of Eqs. (7) and (8), the system describes two strongly interacting modes (modes 1 and 3), coupled just through forward scattering with mode 2. It should not be surprising that the pair of modes (1,3) can be completely gapped out by disorder, as it is not protected even at the single-particle level (we recall, nevertheless, that in the presence of interactions this is possible only for repulsive interactions). Let us assume that the pair (1,3) is indeed completely gapped out. By turning on a small g term, the remaining mode is coupled to the (1,3) pair, which is localized and acts as an electron puddle. The interaction-induced backscattering with the electrons in this effective puddle breaks the topological protection of the single mode 2, as has been shown in Refs. [39] and [40]. Our model reproduces this behavior.

In the next section we discuss the nature of the critical line separating the two neutral massive phases.

VI. TRANSITION BETWEEN PHASES

In the transition between the TRSB and ET phases, the gap in the neutral sector of the system vanishes throughout the whole edge. A theory that describes this one-dimensional gapless system at low energies has an emergent $\mathbb{Z}_3$ symmetry. By going away from the quantum critical point, a gap in the neutral sector opens. By considering a position-dependent interaction that creates the TRSB phase in one segment of the edge while inducing the ET state on the other, we find that a $\mathbb{Z}_3$ parafermion is trapped in the transition region. Below we study the quantum critical point that appears in the transition between these two phases along the edge and how this result implies the existence of nontrivial quasiparticles trapped in domain wall configurations.

A. $\mathbb{Z}_3$ critical theory at the transition

The transition between the TRSB and the ET phase happens at $g + g' = 0$. The amplitude of the cosine terms in the Hamiltonian (14) and (15) vanishes at the transition in the specific line $g = g'$, indicating that along this line of parameters the critical point is Gaussian. By exploring a more general state, e.g., by considering $g \neq g'$ (see also Appendix A), the amplitude of the cosine terms does remain finite. On the transition line $g + g' = 0$, we find that the Luttinger parameters satisfy $K_1 = K_2 = 1$. This implies in particular that the vertex operators made out of fields $\tilde{\theta}_2$ and $\tilde{\varphi}_2$ are both marginally relevant and have the same scaling under RG. The competition between these conjugate fields induces a nontrivial fixed point that corresponds to a CFT of central charge $c = 4/5$.

We introduce the vertex representation of the currents of $\mathrm{SU}(2)_1$ in terms of the field $\tilde{\phi}_{\eta,1}$ [41,42]:

$$J^3_\eta = \eta \frac{\partial_x \tilde{\phi}_{\eta,1}}{\sqrt{2\pi}}, \quad J^{\pm}_\eta = J^1_\eta \pm i J^2_\eta = \frac{e^{\mp i\sqrt{8\pi}\tilde{\phi}_{\eta,1}}}{\sqrt{2\pi}}, \tag{34}$$

which satisfy the Kac-Moody algebra [42] (repeated indices are summed over)

$$\left[J^a_\eta(x), J^b_{\eta'}(y)\right] = \eta \frac{i}{4\pi}\delta'(x-y)\delta^{ab}\delta_{\eta\eta'} + i\epsilon^{abc}J^c_\eta \delta(x-y). \tag{35}$$

Using this representation, it is possible to understand the sector of the Hamiltonian related to the field $\tilde{\phi}_{\eta,1}$ as a critical $\mathrm{SU}(2)_1$ Wess-Zumino-Novikov-Witten (WZNW) model [43–45], perturbed by its primary spin field of scaling dimension $\Delta = \frac{1}{2}$ and a current-current interaction. In particular, defining the primary field of the WZNW as $\sigma(x) = e^{i\sqrt{2\pi}(\tilde{\phi}_{R,1} - \tilde{\phi}_{L,1})}$ the Hamiltonian H becomes

$$\begin{aligned} H = H_{\mathrm{fs}} &+ \pi \frac{g+g'}{(\pi a_0)^2}\int (J^+_R J^-_L + J^-_R J^+_L) \\ &+ \frac{4g}{(\pi a_0)^2}\int [\cos(\sqrt{6\pi}\tilde{\varphi}_2) + \cos(\sqrt{6\pi}\tilde{\theta}_2)](\sigma + \sigma^\dagger), \end{aligned} \tag{36}$$

where H_{fs} contains all the forward-scattering terms of H. The current-current interaction is a marginal perturbation under RG that vanishes at the transition point, while $\sigma(x)$ is relevant. It will open a gap in the $\mathrm{SU}(2)_1$ sector, leaving behind a critical Hamiltonian for the $\tilde{\phi}_{\eta,2}$ fields given by $H \to H_{\mathrm{IR}}$ with

$$\begin{aligned} H_{\mathrm{IR}} = &\frac{v_2}{2}\int dx((\partial_x\tilde{\theta}_2)^2 + (\partial_x\tilde{\phi}_2)^2) \\ &+ \tilde{g}\int dx(\cos(\sqrt{6\pi}\tilde{\varphi}_2) + \cos(\sqrt{6\pi}\tilde{\theta}_2)), \end{aligned} \tag{37}$$

and $\tilde{g}$ a nonuniversal parameter, obtained from the flow of $g\langle\cos(\sqrt{2\pi}\tilde{\varphi}_1)\rangle$ under RG. This theory corresponds to a self-dual sine-Gordon model, which realizes an adiabatic deformation of a $\mathbb{Z}_4$ parafermionic model. This model flows under RG without opening a gap to an IR fixed point given by a $\mathbb{Z}_3$ parafermionic theory [46]. As we have seen before, away from the transition line one of the fields ($\tilde{\theta}_2$ or $\tilde{\varphi}_2$) is locked and develops an energy gap. This implies that by controlling the interactions spatially, it is possible to go across the quantum phase transition between the two different gapped sectors by moving along the edge. By doing so, we find a parafermionic zero mode trapped in the transition region. These zero modes are studied in the next section.

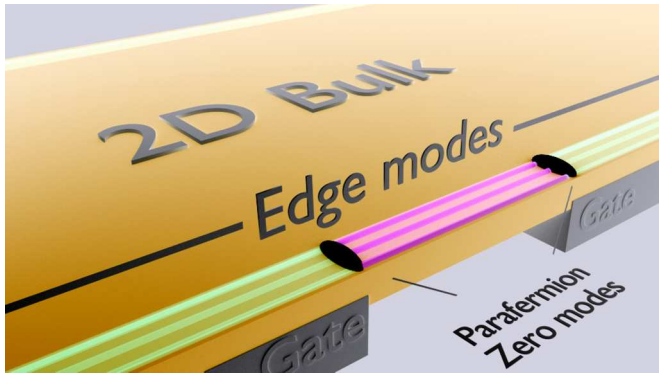

FIG. 6. By changing the interaction strength along the edge, the system transitions from the trivial TRSB phase (depicted in yellow) to the ET phase (depicted in pink). At the boundary between these regions a parafermionic zero mode is localized, represented by the black regions.

B. Parafermionic zero modes

As we have found, the transition between the TRSB and the ET phase is described by a critical theory whose low-energy description is given by a parafermionic CFT of central charge $4/5$ with $\mathbb{Z}_3$ symmetry. By changing the effective interactions between the helical modes along the edge, for example, by external gates, it is possible to generate a domain wall configuration, where on one side the system is in the TRSB phase while on the other it is in the ET phase (see Fig. 6). We can use this result to trap parafermionic quasiparticles in the interface between the two phases in a mechanism similar to the Jackiw-Rebbi fractionalization of the electron [47].

Another mechanism to reveal the presence of these parafermionic modes is by considering a very strong impurity somewhere in the ET region. Although it will renormalize to zero at $T = 0$, there may be an intermediate energy scale below the scale set by the neutral gap Δ_n where the impurity is still strong and in this intermediate regime one can see the parafermionic edge states (cf. the equivalent case for two edges discussed in [48]).

We want to point out that although the existence of parafermions in one-dimensional gapped fermionic systems has been ruled out in [49], their presence in quasi-one-dimensional fermionic gapped systems has been reported in [50–54]. In the system considered here, the edge of the two-dimensional TI remains gapless in the ET phase as the system has collective plasmon modes that can be excited with arbitrarily low energy. This places the edge system discussed in this work in a different category as the quasi-one-dimensional systems mentioned previously. Although in this system is not possible to gap the charge mode without dramatically altering the ET phase (which is shown to be protected against backscattering), it remains a possibility that in similar quasi-one-dimensional systems the charge mode could be gapped while maintaining the appearance of parafermionic modes by the emergence of $c = 4/5$ criticality between two gapped phases. We leave this investigation for the future.

The existence of the gapless charge mode can affect the low-energy theory. It could generate hybridization of the edge modes, lifting the zero modes out of zero energy by the energy that scales inversely with the system size. Under renormalization, this effect corresponds to an irrelevant perturbation that vanishes in the infinite size limit. In this sense, the parafermions that we encounter are not protected, although they appear in a topological phase. Since the charge mode mediates their coupling, it would be interesting to look for situations where the charge mode can be entirely gapped while maintaining the structure in the neutral sector that generates the parafermions.

To develop some intuition into the nature of these zero modes, we introduce an effective description on the lattice, following Ref. [55]. This lattice description captures the physics in the neutral sector qualitatively and contains the symmetries expected to appear around the fixed point obtained from the RG flow of the self-dual Hamiltonian (37), which correspond to $\mathbb{Z}_3$ parafermion CFT.

In general, $\mathbb{Z}_n$ parafermionic modes generalize Majorana fermions, as they satisfy the relations in the lattice

$$\chi_j^n = \eta_j^n = 1, \quad \chi_j^\dagger = \chi_j^{n-1}, \quad \eta_j^\dagger = \eta_j^{n-1}, \tag{38}$$

$$\chi_j \eta_j = \omega \eta_j \chi_j, \tag{39}$$

where j denotes a lattice site and $\omega = e^{2i\pi/n}$. At different lattice sites, the parafermions η, χ satisfy

$$\chi_j \chi_k = \omega \chi_k \chi_j, \quad \eta_j \eta_k = \omega \eta_k \eta_j, \quad \chi_j \eta_k = \omega \eta_k \chi_j, \tag{40}$$

for $j < k$. We are interested in a model that captures the symmetry properties that our system develops in the IR. In particular, the model should display TR and $\mathbb{Z}_3$ symmetry. The simplest model that displays both is given by the three-state quantum Potts model, which in terms of parafermions is given by

$$H_{\text{eff}} = -\sum_{j=1}^{L} h(\chi_j^\dagger \eta_j \bar{\omega} + \text{H.c.}) + J(\eta_j^\dagger \chi_{j+1} \bar{\omega} + \text{H.c.}), \tag{41}$$

with $\bar{\omega}$ the complex conjugate of ω. The parameters h, J are phenomenological and represent a description of the original parameters after renormalization. The phase $\frac{h}{J} \gg 1$ corresponds to the ordered phase. In this case, the spectrum possesses a gap and the ground state spontaneously breaks the $\mathbb{Z}_3$ and TR symmetry. The opposite limit $\frac{h}{J} \ll 1$ corresponds to the disordered phase, which is also gapped but does not break the defining symmetries spontaneously. The point $\frac{h}{J} = 1$ is critical and self-dual. The relation with the microscopic parameters for $g > 0$ and $g' < 0$ is given by

$$\left[\frac{|g'|}{g}\right]_{\text{IR}} \sim \frac{J}{h}, \tag{42}$$

where we denote $[g]_{\text{IR}}$ the renormalized parameter g in the low-energy description. The TRSB phase corresponds to the ordered phase $\frac{h}{J} \gg 1$. (See also the discussion at the end of Appendix A.) In this phase, the low-energy physics is dominated by the Hamiltonian

$$H_{\text{triv}} = -\sum_{j=1}^{N} \frac{h}{J}(\chi_j^\dagger \eta_j \bar{\omega} + \eta_j^\dagger \chi_j \omega). \tag{43}$$

On the other hand, the ET phase corresponds to the limit $\frac{h}{J} \ll 1$, where the Hamiltonian is dominated by

$$H_{\rm top} = -\frac{J}{h}\sum_{j=1}^{N-1}(\eta_j^\dagger \chi_{j+1}\bar{\omega} + \chi_{j+1}^\dagger \eta_j \omega). \tag{44}$$

In this phase, the operators $(\Psi_{\rm in}, \Psi_{\rm out}) \equiv (\chi_1, \eta_N)$ decouple from the Hamiltonian, i.e., $[\Psi_a, H_{\rm top}] = 0$, but they do not commute with the $\mathbb{Z}_3$ symmetry operator Ω, which has a representation

$$\Omega = \prod_{j=1}^{N} \eta_j^\dagger \chi_j, \tag{45}$$

thus satisfying $\Omega\Psi_a = \omega\Psi_a\Omega$. The zero modes map states between different symmetry sectors and are localized at both ends of the topological spatial region.

The TR symmetry $\mathcal{T}$ in this system can be represented as

$$\mathcal{T}\chi_j\mathcal{T}^{-1} = \eta_{N+1-j}, \quad \mathcal{T}\eta_j\mathcal{T}^{-1} = \chi_{N+1-j}, \tag{46}$$

together with the relation $\mathcal{T}i\mathcal{T}^{-1} = -i$ [56].

As we have discussed, the main difference between the ET and the TRSB phase that should be readily accessible in experiments is the value of the conductance. It is then essential to assess the role of disorder in each system. In the next section we analyze the behavior of a single impurity in each of the phases.

VII. DISORDER

For noninteracting electrons, the conductance through the system is given by Landauer formula

$$G = \frac{e^2}{h}\sum_i T_i, \tag{47}$$

where the sum runs over all the transport channels. For the clean system the transmission coefficients $T_i = 1$ such that the total conductance through one edge is $G = 3e^3/h$. In the presence of a static disorder the problem can be solved using the scattering matrix formalism. For a single nonmagnetic impurity of strength $g_{\rm imp}$ the electric conductance is given by (see also Appendix B)

$$G = \frac{e^2}{h}\left[1 + 2\frac{1 - g_{\rm imp}^2}{1 + g_{\rm imp}^2}\right]. \tag{48}$$

The first term on the right-hand side of Eq. (48) follows from a ballistic propagation along the topologically protected channel.

For an interacting system, the Landauer approach, strictly speaking, is not applicable. Nevertheless, one may still use it as a semiqualitative approximation. In this case, one needs to replace the values of transmission coefficients by their renormalized value at energy/temperature T (not to be confused with the transmission coefficients T_i) dependent scale, $g_{\rm imp} \to g_{\rm imp}(T)$. However, Eq. (48) is valid provided that the system remains in a topologically nontrivial state (either inherited or emergent). If topological protection is removed, for example, by a TRSB mechanism, the conductance will generically go to zero.

The backscattering processes are in general proportional to the Fermi momentum components of the order parameters $\mathcal{O}_\alpha^{\rm ord}$ studied previously. Let us model a single pointlike impurity at $x = 0$ that backscatters the helical modes by

$$\mathcal{O}_{\rm imp}(x) = i\delta(x)(L_1^\dagger R_3 - L_3^\dagger R_1) + \text{H.c.} \tag{49}$$

This operator is TR even, so it can be considered as a nonmagnetic impurity. The spatially extended version of this operator corresponds to $\mathcal{O}_5^{\rm ord}$ discussed in Sec. IV. In the bosonic language this operator becomes

$$\mathcal{O}_{\rm imp}(x) = i\delta(x)\left[\bar{\kappa}_1\kappa_3 e^{i\sqrt{2\pi}\tilde{\varphi}_1} - \bar{\kappa}_1\kappa_3 e^{-i\sqrt{2\pi}\tilde{\varphi}_1}\right] \times e^{i\sqrt{\frac{2\pi}{3}}[\sqrt{2}\theta_c + \tilde{\theta}_2]} + \text{H.c.}, \tag{50}$$

where we have written explicitly the Klein factors $\bar{\kappa}_a, \kappa_a$. In the TRSB phase, the fields $(\sqrt{2\pi}\tilde{\varphi}_1^*, \sqrt{6\pi}\tilde{\theta}_2^*)$ are locked into the values $(\pm\frac{2\pi}{3}, 0)$ or $(\pm\frac{\pi}{3}, \pi)$. The spontaneous choice of any of these configurations in the ground state breaks TR symmetry, as the bosonic field $\tilde{\varphi}_1$ is odd under TR. In this case we observe that a nonmagnetic impurity like (49) becomes $\mathcal{O}_{\rm imp} = \delta(x)[\cos(\sqrt{2\pi}\tilde{\varphi}_1^*)\mathcal{O}_+ + \sin(\sqrt{2\pi}\tilde{\varphi}_1^*)\mathcal{O}_-]$, where

$$\mathcal{O}_\pm = ie^{i\frac{\pi}{4}(1\mp1)}[\bar{\kappa}_1\kappa_3 \pm \bar{\kappa}_3\kappa_1]e^{i\sqrt{\frac{2\pi}{3}}[\sqrt{2}\theta_c + \tilde{\theta}_2^*]} + \text{H.c.}, \tag{51}$$

and $\mathcal{T}\mathcal{O}_\pm\mathcal{T}^{-1} = \pm\mathcal{O}_\pm$. This implies that the spontaneous breaking of TR symmetry in the ground state creates an effective magnetic impurity out of a nonmagnetic one. This can be understood as follows: In the TRSB phase the gapless charge mode smears out the TR breaking in the neutral sector, such that there is no true long-range order parameter and just QLRO. By placing a nonmagnetic impurity, the charge mode is locally pinned to a value that minimizes the energy around the impurity. By pinning down the charge around the impurity, the TR breaking of the ground state is revealed and the impurity becomes effectively magnetic.

For temperatures $\Delta_n \ll T \ll \Delta_b$ the charge transport properties of the system are equivalent to the three spinless Luttinger liquids. In this regime a single impurity undergoes the standard Kane-Fisher renormalization [57,58]

$$\frac{dg_{\rm imp}}{d\ell} = (1 - \Delta_{\rm imp})g_{\rm imp}, \tag{52}$$

where $\Delta_{\rm imp} = \frac{K_c}{3} + \frac{K_2}{6} + \frac{1}{2}$ is the scaling dimension of the impurity (49) before the neutral gap is opened. Here $\ell = \ln \Delta_b/T$, where we take the bulk gap Δ_b as the ultraviolet cutoff in this regime. For an impurity with a weak bare value, the conductance in this range of temperatures will be close but below $G = 3e^2/h$, monotonously decreasing as temperature decreases. As the temperature approaches the scale Δ_n, the low-energy fixed point where the neutral modes are gapped starts to control the conductance.

In the TRSB phase, the impurity operator $\mathcal{O}_{\rm imp}$ survives the integration of the massive degrees of freedom and one is left with an effective theory in the gapless charge sector, with the impurity operator now given by

$$\mathcal{O}_{\rm imp} \propto g_{\rm imp}\cos\left(\sqrt{\frac{4\pi}{3}}\theta_c(0)\right). \tag{53}$$

For a sufficiently small amplitude $g_{\rm imp}$, even after the RG flow discussed before, the renormalized value of the impurity

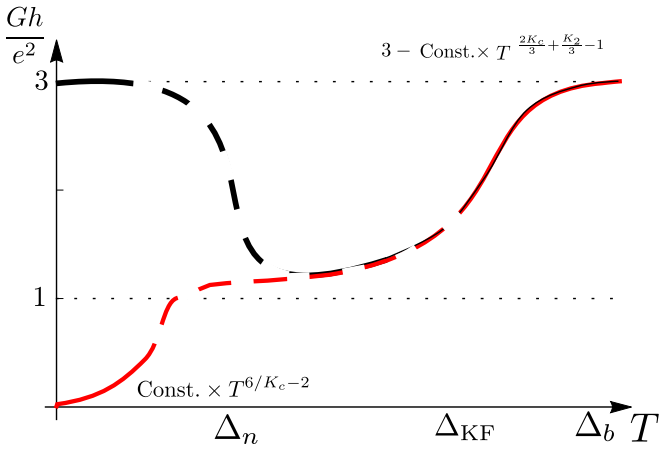

FIG. 7. Schematic plot of electric conductance as a function of temperature in the ET phase (black) and in the TRSB phase (red line). The different energy scales associated with the gap of the two-dimensional TI Δ_b, the gap in the neutral sector on the edge Δ_n, and the scale where the renormalized value of an impurity becomes of order 1 Δ_{KF} determine the behavior of the conductance, with the corresponding exponents shown. The transitions between the different regimes are shown in dashed lines and are just schematic.

strength will remain small such that another Kane-Fisher renormalization analysis can be done. The impurity now scales under RG with the scaling dimension $\Delta = K_c/3$ and an ultraviolet cutoff determined by Δ_n. For any repulsive interaction, it is a strongly relevant perturbation. Thus the impurity strength will flow to a strong coupling fixed point, locking the charge field around the impurity and making the conductance vanish at zero temperature. Note that in the TRSB phase the impurity is effectively magnetic, so Eq. (48) is no longer valid.

We can say something about this strong coupling limit by constructing the leading irrelevant operator that creates a soliton in the θ_c field at this point; i.e., the operator responsible for nonzero current [59,60]. This operator is $\cos[\sqrt{12\pi}\varphi_c(0)]$, which has scaling dimension $d = 3/K_c$, and hence the conductance at low temperature is $G(T) \propto T^{2(d-1)} = T^{6/K_c-2}$.

In contrast, in the ET phase, after the massive degrees of freedom are integrated out, electron and trion backscattering do not contribute. Therefore the conductance of the system in the topological phase at low temperatures is almost perfect, $G \approx 3e^2/h$. In this situation one would usually analyze the approach to perfect conductance in a way similar to above by finding the leading irrelevant operator present after integrating out the massive degrees of freedom. However, the discussion in Sec. V indicates that no such operator exists in the ET phase; hence we expect these corrections not to be a power law. The approach to perfect conductance in the ET phase remains an open question.

We now schematically plot the conductance as a function of temperature for both phases, see Fig. 7. We focus on the limit where the bare value of impurity potential is weak. We assume that the interaction is repulsive and its strength is small, such that all characteristic Luttinger liquid parameters are slightly smaller than 1. Furthermore, we assume for definiteness that the energy scale Δ_{KF} where the impurity becomes strong is higher than the energy scale Δ_n. Just below the two-dimensional TI's gap Δ_b, the conductance in all phases is a nonuniversal function with a value below (but close to) 3 (in the units of e^2/h). As temperature decreases towards the scale Δ_{KF}, the conductance in both phases decreases as $T^{\frac{2K_c}{3}+\frac{K_2}{3}-1}$. Between Δ_{KF} and Δ_n the system behaves as three helical modes in the presence of a nonmagnetic impurity. This signals that the conductance develops a plateau at around $G = 1$. This plateau extends roughly throughout the range of energies between Δ_{KF} and Δ_n. Below Δ_n the conductance in the ET phase starts to rise with decreasing temperature, reaching an ideal limit $G \to 3$ at $T \to 0$. Therefore in this phase, the conductance is a nonmonotonic function of temperature. In the TRSB phase, below the neutral gap, the behavior of the conductance is entirely controlled by an insulating fixed point and the conductance approaches zero as T^{6/K_c-2}.

In the opposite scenario, when $\Delta_n > \Delta_{\mathrm{KF}}$, generically there is no plateau around $G \sim 1$, and the conducting properties of the system are fully dictated by the opening of the neutral gap.

VIII. DISCUSSION AND OUTLOOK

In this paper, we studied the competition of emergent and inherent topological orders. We focused on a system made of three helical wires that may arise as edges states of three copies of two-dimensional topological insulators stacked together or by the edge reconstruction of a single copy. In the noninteracting limit, this system is topologically equivalent to a single helical edge state protected against static disorder. We showed that in the presence of electron interaction this picture changes. We now summarize our findings.

In the presence of interaction, the system may turn into one of two possible states. In the first case, the system acquires a new topological order that cannot be adiabatically connected to the noninteracting one. In the second case, the TR symmetry is spontaneously broken and the system is driven into a topologically trivial state that becomes an Anderson insulator in the presence of a static disorder.

To understand the loss of topological protection, one may take the limit where one of the channels is weakly interacting with the rest. The remaining two channels may be in the topologically trivial or nontrivial state, depending on the interaction strength [24,27]. If two coupled channels happen to be in a topologically trivial state, they would be localized by any finite amount of disorder. Therefore the system of three helical modes effectively becomes equivalent to a single helical channel coupled by hopping to multiple puddles of electronic fluid. Such a system is equivalent to an Anderson insulator [39,40].

The ground state of this topologically trivial state is a strongly correlated one that develops a QLRO. The character of QLRO depends on the details of the interaction. Weak repulsive interaction results in a family of two-particle correlations with power-law decay and $2k_F$ oscillations. For sufficiently strong repulsive interaction $K_c > \sqrt{3}$ and the dominant QLRO is of trionic type.

In the case of small attractive interactions, a new topological order develops. The latter is protected by a gap in the neutral sector that opens inside the one-dimensional system

due to many-body scattering. This state is robust against Anderson localization, with a total conductance of $3e^2/h$ for a moderate disorder.

The transition between topological and nontopological phases occurs along a line in the parameter space of interactions. While the neutral sector of the theory is gapped at both sides of the line, it becomes gapless at the transition. Its low-energy behavior corresponds to the $\mathbb{Z}_3$ parafermionic CFT universality class. The latter is manifested by the emergence of parafermionic excitations at the endpoints of the system.

We also find that the low-energy fixed point has a higher symmetry compared to the interaction between modes that the original model, signaling a *dynamically emergent symmetry*. This phenomenon was previously observed in the context of three leg ladders [61–72]. In our case, the massive phases are ground states of a Hamiltonian that is obtained by marginal deformations of an emergent SU(3) symmetry that is not present in the UV but manifests itself in the IR. The topological phase corresponds to a deformed SU(3) Hamiltonian $\tilde{H}_{\mathrm{SU}(3)}$ of Eq. (20) that can be obtained from the usual SU(3) Gross-Neveu Hamiltonian by performing a chiral transformation. The new topology arises due to a gap in the neutral sector of this Hamiltonian.

Though both symmetry-protected topological order and dynamically generated symmetries were previously known, the current system is an example where both effects act together. The interaction enhances the effective symmetry of the problem in the IR limit. The generated symmetry gives rise to the topologically nontrivial state.

The rich physics of this system invites to further exploration of its different facets. In particular, we consider it crucial to find experimental signatures of parafermions that emerge on the boundary between the phases, to assess their stability in the presence of a gapless charge mode and to account for strong impurities and random disorder. It is appealing to consider how these results generalize to a larger number of helical modes, exploring the possible connection to the theory of interacting symplectic wires. It remains to be seen if the emergent symmetry allows regimes to be found beyond those predicted within a disordered Fermi liquid approach [73]. Finally, from a general perspective, it is compelling to study the general criteria for the existence of dynamically emergent symmetry-protected states.

Note added: Recently we learned about preprints [28,74] with partly overlapping content. The work of Kagalovsky *et al.* [28] discusses TRS breaking in the ground state, leading to zero conductance at zero temperature, for any number of channels $N \geqslant 3$. Our results are in full agreement with theirs for $N = 3$. In this specific case we uncover several nontrivial phases as a function of interaction and crossovers as a function of temperature, which presumably one would see for any odd N, although to confirm or deny this conjecture remains work for the future. The work of Keselman *et al.* [74] looks at a different model, concentrating on $N = 3$ channels in which the noninteracting model is nontopological, and like us, finds a phase with TR symmetry breaking and another phase with an emergent topology. While their TRSB phase is the same one that we find, they curiously find a different emergent topological phase in the universality class of the Haldane spin-1 chain as opposed to our $\mathbb{Z}_3$ parafermionic state. This gapless Haldane state relies on a $(\mathbb{Z}_2)^3$ symmetry, which we explicitly break by the interchain hopping (or equivalently, the splitting of the Fermi points) in our model. In contrast, our parafermion state explicitly emerges from interaction terms that require the interchain tunneling in the Hamiltonian. It remains work for the future to determine the full phase diagram of a more generic $N = 3$ channel system and to see if there are more possibilities for emergent topological states beyond these two.

ACKNOWLEDGMENTS

R.S. would like to thank Eran Sagi, Jinhong Park, and Benjamin Béri for stimulating discussions. D.G. was supported by ISF Grant No. 584/14 and the Israeli Ministry of Science, Technology and Space. R.S. acknowledges funding from from the EPSRC through Grant No. EP/M02444X/1 and an ERC Starting Grant, No. 678795 TopInSy.

APPENDIX A: GENERAL MODEL OF THREE HELICAL MODES

We now extend the discussion of our model for the case of general interactions between nonidentical helical states. We assume that the system consists of three quantum-spin-Hall insulators stacked in parallel such that the asymmetry between the edge modes is not too big, i.e., the parameters of all the modes are approximately equal. In this case, TR symmetry implies that the dispersion relations for the edge modes $E_a^\eta(k)$ satisfy $E_a^\eta(k) = E_a^{-\eta}(-k)$. We consider first the case of modes with the same Fermi velocity and general interactions.

1. Equal Fermi velocities

Using the same notation as the main text, we consider three helical modes described by the fermion destruction operator of momentum k, $c_{k,a}^\eta$, where $a = (1, 2, 3)$ denotes the mode and $\eta = (+, -)$ labels its helicity. For small momenta, the noninteracting Hamiltonian is

$$H_0 = \sum_{k,a,\eta} \eta v_F k \left(c_{k,a}^\eta\right)^\dagger c_{k,a}^\eta + \alpha_{so} k \left(c_{k,a}^\eta\right)^\dagger c_{k,a}^{\bar{\eta}} - \sum_{k,\eta} \left(t_L \left(c_{k,2}^\eta\right)^\dagger c_{k,1}^\eta + t_R \left(c_{k,2}^\eta\right)^\dagger c_{k,3}^\eta + \mathrm{H.c.}\right), \quad \text{(A1)}$$

where v_F is the Fermi velocity of the modes, and α_{so} parameterizes a residual spin-orbit coupling along the edge. We assume that tunneling only occurs between the modes which are closest in space, with amplitudes t_L and t_R. A diagram of the arrangement of helical modes and their labeling is given in Fig. 8.

The energy dispersion relations in the band basis are $E_\eta^a = \eta \tilde{v}_F k + \lambda_a t_\perp$, with the new Fermi velocity $\tilde{v}_F = \sqrt{v_F^2 + \alpha_{so}^2}$, the perpendicular tunneling parameter $t_\perp = \sqrt{t_L^2 + t_R^2}$, and $\lambda_a = (-1, 0, 1)$. The single-particle Hamiltonian is invariant under the symmetry of interchanging the modes $1 \leftrightarrow 3$ and $t_L \leftrightarrow t_R$.

Going from the original modes to the band modes that diagonalize the Hamiltonian is implemented by the unitary

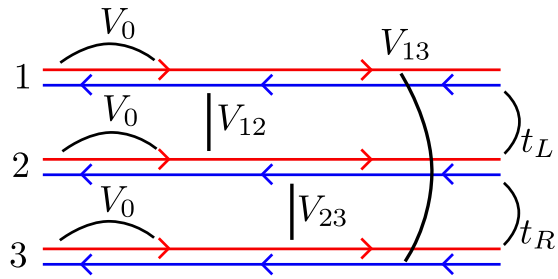

FIG. 8. Generic diagram of three helical modes. We label the different channels by 1, 2, and 3 and the different interaction strengths as depicted. Tunneling amplitude between mode 1 and 2 is denoted t_L, while tunneling between 2 and 3 is denoted t_R. Tunneling between modes 1 and 3 is assumed to be negligible.

transformation $[U(v)]^{\eta\eta'}_{ab} = (U_c(v))_{ab}(U_h)^{\eta\eta'}$, where $\tan v = \frac{t_L}{t_R}$. The unitary transformation $U_h = e^{i\beta\sigma_y}$ (with $\tan 2\beta = \frac{\alpha_{so}}{v_F}$) acts on the helicities, while U_c acts in the channel index rotating the modes into the band basis and is given by

$$U_c(v) = \frac{1}{\sqrt{2}}\begin{pmatrix} \sin v & -1 & \cos v \\ \sqrt{2}\cos v & 0 & -\sqrt{2}\sin v \\ \sin v & 1 & \cos v \end{pmatrix}. \tag{A2}$$

A generic interaction between the three different helical modes is described by the following Hamiltonian:

$$H_{\rm int} = \sum_{i,a} V_0 n_{i,a} n_{i,a} + \sum_{i,a\neq b} V_{ab} n_{i,a} n_{i,b}, \tag{A3}$$

where the density at each site i and channel a is $n_{i,a} = \sum_\sigma (c^\sigma_{i,a})^\dagger c^\sigma_{i,a}$. These interaction parameters are symmetric, $V_{ab} = V_{ba}$.

After bosonization, using the basis (11) of the main text, the forward-scattering Hamiltonian becomes

$$H_{\rm fs} = \sum_{a=c,1,2} \frac{v_a}{2} \int dx \left(K_a (\partial_x \tilde{\varphi}_2)^2 + \frac{1}{K_a} (\partial_x \tilde{\theta}_2)^2 \right) + \int dx (\zeta_1 \partial_x \tilde{\varphi}_c \partial_x \tilde{\varphi}_2 + \zeta_2 \partial_x \tilde{\theta}_c \partial_x \tilde{\theta}_2), \tag{A4}$$

where the parameters $v_a, K_a, \zeta_{1,2}$ satisfy $v_1 = \tilde{v}_F - \frac{g_2}{4\pi} + \frac{g-g'}{2\pi}$, $K = 1$, $\zeta_1 = \frac{\sqrt{2}}{6\pi}(g'-g)$, $\zeta_2 = \frac{\sqrt{2}}{6\pi}(3g - g_1 - g')$, and

$$v_2 K_2 = \tilde{v}_F - \frac{g_2}{4\pi} + \frac{g'-g}{6\pi}, \tag{A5}$$

$$v_2 K_2^{-1} = \tilde{v}_F - \frac{g_2}{4\pi} + \frac{g}{2\pi} + \frac{5g'}{6\pi} - \frac{2g_1}{3\pi}, \tag{A6}$$

$$v_c K_c = \tilde{v}_F + \frac{g_2}{2\pi} + \frac{g'-g}{3\pi}, \tag{A7}$$

$$v_c K_c^{-1} = \tilde{v}_F + \frac{g_2}{2\pi} + \frac{2(g'+g_1)}{3\pi} + \frac{g+3\tilde{V}_0}{\pi}. \tag{A8}$$

In terms of the microscopic parameters, we have the relations $\tilde{V}_0 = \frac{a_0}{4}(V_0 + V_{12} + V_{13} + V_{23})$ and

$$\frac{g}{a_0} = \frac{V_0 - V_{13}}{8}(1 + \cos^2 2v) + \frac{V_{23} - V_{12}}{4}\cos 2v,$$

$$\frac{g'}{a_0} = \frac{V_0 + V_{13} - V_{23} - V_{12}}{4} + \frac{V_0 - V_{13}}{2}\cos^2 2v,$$

$$\frac{g_1}{a_0} = \frac{\cos 2v}{2}[V_{12} - V_{23} - (V_0 - V_{13})\cos 2v], \tag{A9}$$

$$g_2 = 2(2g + g_1), \quad \text{and} \quad g_1' = 2(g' - g) + g_2. \tag{A10}$$

The complete Hamiltonian reads

$$H = H_{\rm fs} + \bar{g}_1' \int dx \cos(2\sqrt{2\pi}\tilde{\varphi}_1) + 2\bar{g}_2 \int dx [\cos(\sqrt{6\pi}\tilde{\varphi}_2) + \cos(\sqrt{6\pi}\tilde{\theta}_2)] \cos(\sqrt{2\pi}\tilde{\varphi}_1), \tag{A11}$$

with $\bar{g} = \frac{g}{2(\pi a_0)^2}$. The transition line between the ET and TRSB phases is defined by $g + g' - g_1 = 0$. The symmetric limit $t_L = t_R$ corresponds to $v = \pi/4$. For this value, the general model reduces to the one we used in the main part of the manuscript. Assuming that $g_1 > 0$, we can define $\chi = \frac{g+g'}{g_1}$ and use this parameter to characterize the transition between the TRSB and the ET phase. In this case, $\chi > 1$ implies that the system flows into the TRSB phase, while $\chi < 1$ implies that the system flows to the ET phase. The renormalized parameter $[\chi]_{\rm IR}$ obtained from the RG flow of the interaction constants g, g', g_1 determines the properties of the low-energy theory, so it takes the role of h/J in the Hamiltonian $H_{\rm eff}$ of Eq. (41). A similar analysis can be done in the regime where $g_1 < 0$. For $g_1 = 0$, the system is always in the TRSB phase if $g + g' > 0$, while if $g + g' < 0$ the system is always in the ET phase. To obtain a transition in this case, the parameters g, g' should have opposite signs. The case $g > 0, g' < 0$ is discussed in the main text. The opposite case of $g' > 0, g < 0$ can be obtained from the previous one by interchanging the roles of g and g'.

2. Different Fermi velocities and general interedge tunneling

A system of three helical modes can be realized not only by stacking of the nearly identical TIs, but also through the edge reconstruction [32,33,75]. In all these cases the helical modes are not necessarily identical. Furthermore, general tunneling and spin-orbit interaction between all the modes can produce Fermi points that are not equally spaced, together with different Fermi velocities after linearization of the momenta around the Fermi points. In this case, the only operator that is affected is $\mathcal{O}_{123} \equiv \int dx (L_1^\dagger L_2 R_2^\dagger R_3 + L_2^\dagger L_3 R_1^\dagger R_2 + \text{H.c.})$. It acquires a finite mismatch of the Fermi momenta $\Delta k_F = k_F^1 + k_F^3 - 2k_F^2$. Nevertheless, as long as the incommensurability is small in comparison with the gap in the neutral sector, i.e., $\bar{v_F}\Delta k_F < \Delta_n$, our results remain unchanged. Here $\bar{v_F}$ is the average Fermi velocity. This condition follows from repeating the steps of RG analysis and is similar to the one that arises in the context of commensurable incommensurable transitions in one dimension [34]. If the condition $\bar{v_F}\Delta k_F < \Delta_n$ is satisfied,

the differences in Fermi velocities correspond to irrelevant perturbations [76] and do not affect the results for moderate velocity differences.

APPENDIX B: SCATTERING MATRIX FOR NONINTERACTING CHANNELS

The Schrödinger equation for three chiral fermions scattering off an impurity at $x = 0$ can be written as

$$iv_F(1 \otimes \sigma_z)\partial_x\Psi + \mathcal{V}\delta(x)\Psi = E\Psi. \tag{B1}$$

Here $\mathcal{V}$ parameterizes the scatterer and Ψ is a six-component spinor that contains the right and left mover part of the chiral fermion. This scatterer potential can be decomposed in the basis $V = \sum_a V_a \otimes \sigma^a$, where σ^a are the Pauli and the 2×2 identity matrices. The matrices V_a act in the channel space, while σ^a acts between the chiralities of the fermions. Without losing generality, the backscattering part of the potential can be written in the form $V_x \otimes \sigma_x$, where TR symmetry dictates that the scatterer potential V is such that $V_x^T = -V_x$. Taking the determinant of this equation, we find that $\det(V_x^T) = (-1)^3 \det(V_x) = 0$. It also follows from the antisymmetry of V_x that its trace vanishes. In the basis $\tilde{\Psi} = (U_V \otimes 1_{2\times 2})\Psi$ that diagonalizes V_x Eq. (B1) splits into

$$\begin{aligned} iv_F(1 \otimes \sigma_z)\partial_x\tilde{\Psi}_1 + ir\sigma_x\delta(x)\tilde{\Psi}_1 &= E\tilde{\Psi}_1\,, \\ iv_F(1 \otimes \sigma_z)\partial_x\tilde{\Psi}_2 &= E\tilde{\Psi}_2\,, \\ iv_F(1 \otimes \sigma_z)\partial_x\tilde{\Psi}_3 - ir\sigma_x\delta(x)\tilde{\Psi}_3 &= E\tilde{\Psi}_3\,, \end{aligned} \tag{B2}$$

where r is one of the eigenvalues of V_x and parameterizes the strength of the scattering potential. These equations describe the propagation of three decoupled modes that constitute independent conducting channels. Due to TR symmetry and the number of channels being odd, there is one mode with zero reflection across the impurity. Solving the previous equations using the regularization $\int dx\delta(x)\Psi(0) = \frac{1}{2}[\Psi(0_+) + \Psi(0_-)]$, we find the scattering matrix for modes 1 and 3 to be

$$S = \cos\beta\sigma^0 \pm i\sin\beta\sigma^x, \tag{B3}$$

where the $+(-)$ sign is for the mode 1(3). Here $\beta = 2\tan^{-1}\frac{r}{2v_F}$. Defining $g_{\text{imp}} \equiv \frac{r}{2v_F}$, it is found [77] that the transmission coefficient T_i for mode 1 and 3 is

$$T_1 = T_3 = \frac{1 - g_{\text{imp}}^2}{1 + g_{\text{imp}}^2}. \tag{B4}$$

[1] D. Thouless, *Topological Quantum Numbers in Nonrelativistic Physics* (World Scientific, Singapore, 1998).

[2] F. D. M. Haldane, Nobel lecture: Topological quantum matter, Rev. Mod. Phys. **89**, 040502 (2017).

[3] G. Volovik, *The Universe in a Helium Droplet*, International Series of Monographs on Physics (Cambridge University Press, Cambridge, UK, 2013).

[4] D. J. Thouless, M. Kohmoto, M. P. Nightingale, and M. den Nijs, Quantized Hall Conductance in a Two-Dimensional Periodic Potential, Phys. Rev. Lett. **49**, 405 (1982).

[5] D. C. Tsui, H. L. Stormer, and A. C. Gossard, Two-Dimensional Magnetotransport in the Extreme Quantum Limit, Phys. Rev. Lett. **48**, 1559 (1982).

[6] R. B. Laughlin, Anomalous Quantum Hall Effect: An Incompressible Quantum Fluid with Fractionally Charged Excitations, Phys. Rev. Lett. **50**, 1395 (1983).

[7] C. L. Kane and E. J. Mele, Z_2 Topological Order and the Quantum Spin Hall Effect, Phys. Rev. Lett. **95**, 146802 (2005).

[8] B. A. Bernevig, T. L. Hughes, and S.-C. Zhang, Quantum spin Hall effect and topological phase transition in HgTe quantum wells, Science **314**, 1757 (2006).

[9] B. A. Bernevig and S.-C. Zhang, Quantum Spin Hall Effect, Phys. Rev. Lett. **96**, 106802 (2006).

[10] X.-L. Qi, T. L. Hughes, and S.-C. Zhang, Topological field theory of time-reversal invariant insulators, Phys. Rev. B **78**, 195424 (2008).

[11] M. König, S. Wiedmann, C. Brüne, A. Roth, H. Buhmann, L. W. Molenkamp, X.-L. Qi, and S.-C. Zhang, Quantum spin Hall insulator state in HgTe quantum wells, Science **318**, 766 (2007).

[12] L. Fu and C. L. Kane, Topological insulators with inversion symmetry, Phys. Rev. B **76**, 045302 (2007).

[13] L. Fu, C. L. Kane, and E. J. Mele, Topological Insulators in Three Dimensions, Phys. Rev. Lett. **98**, 106803 (2007).

[14] L. Fu and C. L. Kane, Superconducting Proximity Effect and Majorana Fermions at the Surface of a Topological Insulator, Phys. Rev. Lett. **100**, 096407 (2008).

[15] D. Hsieh, D. Qian, L. Wray, Y. Xia, Y. S. Hor, R. J. Cava, and M. Z. Hasan, A topological dirac insulator in a quantum spin Hall phase, Nature (London) **452**, 970 (2008).

[16] D. Hsieh, Y. Xia, L. Wray, D. Qian, A. Pal, J. H. Dil, J. Osterwalder, F. Meier, G. Bihlmayer, C. L. Kane, Y. S. Hor, R. J. Cava, and M. Z. Hasan, Observation of unconventional quantum spin textures in topological insulators, Science **323**, 919 (2008).

[17] M. Z. Hasan and C. L. Kane, Topological insulators, Rev. Mod. Phys. **82**, 3045 (2010).

[18] M. König, H. Buhmann, L. W. Molenkamp, T. Hughes, C.-X. Liu, X.-L. Qi, and S.-C. Zhang, The quantum spin Hall efect: Theory and experiment, J. Phys. Soc. Jpn. **77**, 031007 (2008).

[19] A. Roth, C. Brüne, H. Buhmann, L. W. Molenkamp, J. Maciejko, X. L. Qi, and S. C. Zhang, Nonlocal transport in the quantum spin Hall state, Science **325**, 294 (2009).

[20] A. Kitaev, Periodic table for topological insulators and superconductors, AIP Conf. Proc. **1134**, 22 (2009).

[21] S. Ryu, A. P. Schnyder, A. Furusaki, and A. Ludwig, Topological insulators and superconductors: Tenfold way and dimensional hierarchy, New J. Phys. **12**, 065010 (2010).

[22] L. Fidkowski and A. Kitaev, Effects of interactions on the topological classification of free fermion systems, Phys. Rev. B **81**, 134509 (2010).

[23] R. A. Santos and D. B. Gutman, Interaction-protected topological insulators with time reversal symmetry, Phys. Rev. B **92**, 075135 (2015).

[24] R. A. Santos, D. B. Gutman, and S. T. Carr, Phase diagram of two interacting helical states, Phys. Rev. B **93**, 235436 (2016).

[25] N. Kainaris, R. A. Santos, D. B. Gutman, and S. T. Carr, Interaction induced topological protection in one-dimensional conductors, Fortschr. Phys. **65**, 1600054 (2017).
[26] A. Keselman and E. Berg, Gapless symmetry-protected topological phase of fermions in one dimension, Phys. Rev. B **91**, 235309 (2015).
[27] N. Kainaris and S. T. Carr, Emergent topological properties in interacting one-dimensional systems with spin-orbit coupling, Phys. Rev. B **92**, 035139 (2015).
[28] V. Kagalovsky, A. L. Chudnovskiy, and I. V. Yurkevich, Stability of a topological insulator: Interactions, disorder and parity of Kramers doublets, Phys. Rev. B **97**, 241116 (2018).
[29] J. T. Chalker and A. Dohmen, Three-Dimensional Disordered Conductors in a Strong Magnetic Field: Surface States and Quantum Hall Plateaus, Phys. Rev. Lett. **75**, 4496 (1995).
[30] L. Balents and M. P. A. Fisher, Chiral Surface States in the Bulk Quantum Hall Effect, Phys. Rev. Lett. **76**, 2782 (1996).
[31] S. H. Kim, K. H. Jin, J. Park, J. S. Kim, S. H. Jhi, and H. W. Yeom, Topological phase transition and quantum spin Hall edge states of antimony few layers, Sci. Rep. **6**, 33193 (2016).
[32] D. B. Chklovskii, B. I. Shklovskii, and L. I. Glazman, Electrostatics of edge channels, Phys. Rev. B **46**, 4026 (1992).
[33] J. Wang, Y. Meir, and Y. Gefen, Spontaneous Breakdown of Topological Protection in Two Dimensions, Phys. Rev. Lett. **118**, 046801 (2017).
[34] T. Giamarchi, *Quantum Physics in One Dimension*, International Series of Monographs on Physics (Clarendon Press, Oxford, 2003).
[35] A. O. Gogolin, A. A. Nersesyan, and A. M. Tsvelik, *Bosonization and Strongly Correlated Systems* (Cambridge University Press, Cambridge, UK, 2004).
[36] D. J. Gross and A. Neveu, Dynamical symmetry breaking in asymptotically free field theories, Phys. Rev. D **10**, 3235 (1974).
[37] G. B. Arfken and H. J. Weber, *Mathematical Methods for Physicists*, 4th ed., edited by G. B. Arfken and H. J. Weber (Academic Press, Boston, 1995), pp. 223–283.
[38] R. Landauer, Spatial variation of currents and fields due to localized scatterers in metallic conduction, IBM J. Res. Dev. **1**, 223 (1957).
[39] J. I. Väyrynen, M. Goldstein, and L. I. Glazman, Helical Edge Resistance Introduced by Charge Puddles, Phys. Rev. Lett. **110**, 216402 (2013).
[40] J. I. Väyrynen, M. Goldstein, Y. Gefen, and L. I. Glazman, Resistance of helical edges formed in a semiconductor heterostructure, Phys. Rev. B **90**, 115309 (2014).
[41] P. Di Francesco, P. Mathieu, and D. Sénéchal, *Conformal Field Theory*, Graduate Texts in Contemporary Physics (Springer, New York, 1997).
[42] E. Fradkin, *Field Theories of Condensed Matter Physics* (Oxford Science Publications, Oxford, UK, 2009).
[43] J. Wess and B. Zumino, Consequences of anomalous ward identities, Phys. Lett. B **37**, 95 (1971).
[44] S. P. Novikov, The Hamiltonian formalism and a many-valued analog of Morse theory, Russ. Math. Surv. **37**, 1 (1982).
[45] E. Witten, Global aspects of current algebra, Nucl. Phys. B **223**, 422 (1983).
[46] P. Lecheminant, A. O. Gogolin, and A. A. Nersesyan, Criticality in self-dual sine-Gordon models, Nucl. Phys. B **639**, 502 (2002).
[47] R. Jackiw and C. Rebbi, Solitons with fermion number $\frac{1}{2}$, Phys. Rev. D **13**, 3398 (1976).
[48] N. Kainaris, S. T. Carr, and A. D. Mirlin, Transmission through a potential barrier in luttinger liquids with a topological spin gap, Phys. Rev. B **97**, 115107 (2018).
[49] L. Fidkowski and A. Kitaev, Topological phases of fermions in one dimension, Phys. Rev. B **83**, 075103 (2011).
[50] Y. Oreg, E. Sela, and A. Stern, Fractional helical liquids in quantum wires, Phys. Rev. B **89**, 115402 (2014).
[51] J. Klinovaja and D. Loss, Time-reversal invariant parafermions in interacting Rashba nanowires, Phys. Rev. B **90**, 045118 (2014).
[52] J. Klinovaja and D. Loss, Parafermions in an Interacting Nanowire Bundle, Phys. Rev. Lett. **112**, 246403 (2014).
[53] A. M. Tsvelik, Integrable Model with Parafermion Zero Energy Modes, Phys. Rev. Lett. **113**, 066401 (2014).
[54] L.-W. Yu and M.-L. Ge, $\mathbb{Z}_3$ parafermionic chain emerging from Yang-Baxter equation, Sci. Rep. **6**, 21497 (2016).
[55] P. Fendley, Parafermionic edge zero modes in $\mathbb{Z}_n$-invariant spin chains, J. Stat. Mech. (2012) P11020.
[56] R. S. K. Mong, D. J. Clarke, J. Alicea, N. H. Lindner, P. Fendley, C. Nayak, Y. Oreg, A. Stern, E. Berg, K. Shtengel, and M. P. A. Fisher, Universal Topological Quantum Computation from a Superconductor-Abelian Quantum Hall Heterostructure, Phys. Rev. X **4**, 011036 (2014).
[57] C. L. Kane and M. P. A. Fisher, Transport in a One-Channel Luttinger Liquid, Phys. Rev. Lett. **68**, 1220 (1992).
[58] C. L. Kane and M. P. A. Fisher, Impurity scattering and transport of fractional quantum Hall edge states, Phys. Rev. B **51**, 13449 (1995).
[59] H. Saleur, Topological Aspects of Low Dimensional Systems, in *Proceedings, Les Houches Summer School of Theoretical Physics* (Springer, Berlin, 1999).
[60] S. T. Carr, B. N. Narozhny, and A. A. Nersesyan, Spinful fermionic ladders at incommensurate filling: Phase diagram, local perturbations, and ionic potentials, Ann. Phys. **339**, 22 (2013).
[61] P. Lecheminant, P. Azaria, E. Boulat, S. Capponi, G. Roux, and S. R. White, Trionic and quarteting phase in one-dimensional multicomponent ultracold fermions, Int. J. Mod. Phys. E **17**, 2110 (2008).
[62] Á. Rapp, W. Hofstetter, and G. Zaránd, Trionic phase of ultracold fermions in an optical lattice: A variational study, Phys. Rev. B **77**, 144520 (2008).
[63] P. Azaria, Fractionalization in three-component fermionic atomic gases in a one-dimensional optical lattice, arXiv:1011.2944.
[64] P. Lecheminant and H. Nonne, Exotic quantum criticality in one-dimensional coupled dipolar bosons tubes, Phys. Rev. B **85**, 195121 (2012).
[65] J. Pohlmann, A. Privitera, I. Titvinidze, and W. Hofstetter, Trion and dimer formation in three-color fermions, Phys. Rev. A **87**, 023617 (2013).
[66] Y. Okanami, N. Takemori, and A. Koga, Stability of the superfluid state in three-component fermionic optical lattice systems, Phys. Rev. A **89**, 053622 (2014).
[67] A. Sotnikov, Critical entropies and magnetic-phase-diagram analysis of ultracold three-component fermionic mixtures in optical lattices, Phys. Rev. A **92**, 023633 (2015).

[68] Y. Nishida, Polaronic Atom-Trimer Continuity in Three-Component Fermi Gases, Phys. Rev. Lett. **114**, 115302 (2015).

[69] G. Klingschat and C. Honerkamp, Exact diagonalization study of trionic crossover and trion liquid in the attractive three-component Hubbard model, Phys. Rev. B **82**, 094521 (2010).

[70] S. Miyatake, K. Inaba, and S. I. Suga, Color-selective Mott transition and color superfluid of three-component fermionic atoms with repulsive interaction in optical lattices, Phys. C (Amsterdam, Neth.) **470**, S916 (2010).

[71] T. Ozawa and G. Baym, Population imbalance and pairing in the BCS-BEC crossover of three-component ultracold fermions, Phys. Rev. A **82**, 063615 (2010).

[72] P. Azaria, Bound-state dynamics in one-dimensional multi-species fermionic systems, Phys. Rev. B **95**, 125106 (2017).

[73] A. M. Finkelstein, *Electron Liquid in Disordered Conductors*, Soviet Scientific Reviews Vol. 14 (Harwood Academic Publishers, GmbH, London, 1990).

[74] A. Keselman, E. Berg, and P. Azaria, From one-dimensional charge conserving superconductors to the gapless Haldane phase, Phys. Rev. B **98**, 214501 (2018).

[75] C. de C. Chamon and X. G. Wen, Sharp and smooth boundaries of quantum Hall liquids, Phys. Rev. B **49**, 8227 (1994).

[76] M. Fabrizio, Role of transverse hopping in a two-coupled-chains model, Phys. Rev. B **48**, 15838 (1993).

[77] B. H. J. McKellar and G. J. Stephenson, Klein paradox and the Dirac-Kronig-Penney model, Phys. Rev. A **36**, 2566 (1987).